Mathematical models on the impact of noise and dyadic molecular structures on the properties of a cardiac myocyte

Antti Juho Tanskanen

Department of Mathematics and Statistics, Faculty of Science
University of Helsinki

Academic dissertation

To be presented, with the permission of the Faculty of Science of the University of Helsinki, for public criticism in Auditorium XII, the Main Building of the University, on May 15th, 2008, at 12 noon

Correspondence
antti.tanskanen@iki.fi

ISBN 978-952-92-3730-2 (paperback)
Helsinki University Printing House

ISBN 978-952-10-4653-7 (PDF)
http://ethesis.helsinki.fi/

Helsinki, 2008

Abstract

In cardiac myocytes (heart muscle cells), coupling of electric signal known as the action potential to contraction of the heart depends crucially on calcium-induced calcium release (CICR) in a microdomain known as the dyad. During CICR, the peak number of free calcium ions (Ca^{2+}) present in the dyad is small, typically estimated to be within range 1-100. Since the free Ca^{2+} ions mediate CICR, noise in Ca^{2+} signaling due to the small number of free calcium ions influences Excitation-Contraction (EC) coupling gain. Noise in Ca^{2+} signaling is only one noise type influencing cardiac myocytes, e.g., ion channels playing a central role in action potential propagation are stochastic machines, each of which gates more or less randomly, which produces gating noise present in membrane currents. How various noise sources influence macroscopic properties of a myocyte, how noise is attenuated and taken advantage of are largely open questions. In this thesis, the impact of noise on CICR, EC coupling and, more generally, macroscopic properties of a cardiac myocyte is investigated at multiple levels of detail using mathematical models. Complementarily to the investigation of the impact of noise on CICR, computationally-efficient yet spatially-detailed models of CICR are developed. The results of this thesis show that (1) gating noise due to the high-activity mode of L-type calcium channels playing a major role in CICR may induce early after-depolarizations associated with polymorphic tachycardia, which is a frequent precursor to sudden cardiac death in heart failure patients; (2) an increased level of voltage noise typically increases action potential duration and it skews distribution of action potential durations toward long durations in cardiac myocytes; and that (3) while a small number of Ca^{2+} ions mediate CICR, Excitation-Contraction coupling is robust against this noise source, partly due to the shape of ryanodine receptor protein structures present in the cardiac dyad.

Keywords: cardiac myocyte, calcium-induced calcium release, excitation-contraction coupling, noise, mathematical modeling, early-afterdepolarization

Acknowledgements

This thesis is a result of my stay at the Center for Cardiovascular Bioinformatics and Modeling at Johns Hopkins University, which was kindly enabled by Dr. Raimond Winslow. Nevertheless, this thesis would not have seen the light of day without encouragement and help from Drs Elja Arjas and Mats Gyllenberg. I must also thank Drs Joe Greenstein and Luis Alvarez, who co-authored articles included in this thesis.

I am grateful to Drs Bernt Øksendal and, in particular, Juha Voipio for critical review of this thesis and giving many valuable advice and suggestions.

I express my gratitude to my parents for continuous encouragement and support. But most of all I am indebted to Eija for years of love, patience and understanding. Finally, I thank Elsa and Lauri for solving any problems in deciding what to do with my free time. You guys will never cease to amaze me.

Helsinki, April 2008

Contents

List of publications

This thesis is based on the following original articles, which are referred to in the Introduction by Roman numerals I-IV.

I Tanskanen A.J., Greenstein J.L., O'Rourke B., Winslow R.L., 2005. The role of stochastic and modal gating of cardiac L-type Ca^{2+} channels on early after-depolarizations. Biophysical Journal 88: 85-95.

II Tanskanen A.J., Alvarez L.H.R., 2007. Voltage noise influences action potential duration in cardiac myocytes. Mathematical Biosciences 208: 125-146.

III Tanskanen A.J., Greenstein J.L., Chan M., Sun X., Winslow R.L., 2007. Protein geometry and placement in the cardiac dyad influence macroscopic properties of calcium-induced calcium-release. Biophysical Journal 92: 3379-3396.

IV Tanskanen A.J., Winslow R.L., 2006. Integrative structurally detailed model of calcium dynamics in the cardiac diad. SIAM Multiscale: Modeling and Simulation 5: 1280-1296.

Author's contribution

In article I, the author is responsible for finding (really, stumbling upon) stochastically occurring early after-depolarizations in a myocyte model, performing and implementing the numerical simulations, and analyzing the results. In article II, the author formulated the explored models, created and analyzed the numerical models, partially worked out the proofs and derivations, and wrote the article. In article III, the author formulated the model and partially the method, wrote simulation code, and made the initial simulations. In article IV, the author is responsible for the method, simulations, and writing. The introduction is written entirely by the author.

Chapter 1

Introduction

1.1 Motivation

Noise has many roles in cellular biology, including noise-induced amplification of signals [76], generation of errors in DNA replication [54], and enhancement of neuron spiking reliability [102]. Often linked to detrimental consequences (e.g., mutations leading to various diseases), noise also has beneficial roles, e.g., evolution is partly a result of noisy copying of DNA. While cellular processes take place in a fluctuating environment, cells behave in a surprisingly orderly way. How this order arises from noise, and how noise is attenuated and taken advantage of in cellular processes are largely open questions [74].

Calcium (Ca^{2+}) is a ubiquitous second messenger in many cellular processes [10]. In the cardiac myocytes (heart muscle cells), its role is crucial as a part of the Excitation-Contraction (EC) coupling: Ca^{2+} translates electrical signal known as the action potential (AP) to a contraction of the heart. Abnormalities of Ca^{2+} dynamics in cardiac myocytes may have severe consequences. For example, mutations in a gene encoding Ca^{2+}-sensitive Ca^{2+}-release channels (known as ryanodine receptors, or RyRs) account for two-thirds of an inherited heart disorder known as Catecholaminergic polymorphic ventricular tachycardia [51].

While large amount of data on cellular properties is available, it is commonly acknowledged that data alone is not sufficient to explain emergent properties arising from complex interplay of biochemical networks [105]. Quantitative description of intracellular Ca^{2+} dynamics is best accomplished by integrative modeling, that is, models that couple experimental data to interaction networks and thereby to function of active biological entities. Recent advances in mathematical (e.g., Astala and Päivärinta [6]), experimental (e.g., Sharma et al. [80]) and computational (e.g., Bader, 2004)

methods, as well as the availability of large quantities of data [96] all drive the advancement of computational cardiobiology, which has become an important tool in decoding particulars of the operation of the heart, as shown by extensive literature documenting both the reconstructive and predictive abilities of integrative models of excitable cells [105, 44].

The ultimate aim of computational cardiobiology is to describe the functioning of an entire heart from the first principles. Incorporating integrative, biophysically detailed single-cell models into a computational model of the whole heart is still at an early stage of development, but it is essential to an attempt to understand heart arrhythmias [64, 65]. This kind of computational approach to modeling whole organs starting from models of individual cells is known as integrative whole-heart modeling, and it has only recently become feasible [44].

From the viewpoint of mathematical modeling, a cardiac myocyte is a stochastic high-dimensional dynamical system with strong feedback and a significant noise component. In this thesis, mathematical methods are applied to model isolated cardiac myocytes, with particular emphasis on integrative models in which noise is present. The aim of this thesis is (1) to investigate the role of noise on macroscopic properties of a cardiac myocyte; (2) to study the role of noise on dyadic Ca^{2+} dynamics; and (3) to examine Ca^{2+} dynamics in cardiac myocytes at multiple levels of detail, which together provide a multiscale view.

1.2 Organization of this thesis

This thesis is divided into two parts: (1) a review of the relevant biology and the mathematical methods of myocyte modeling; and (2) four published articles. Part (1) consists of a brief review of the relevant cardiobiology (chapter 2), a review of electrophysiological models of excitable cells (chapter 3), examination of Ca^{2+}-induced Ca^{2+} release in the dyad (chapter 4), investigation of the role of noise on cardiac myocytes (section 5), and a discussion of the results of the four original articles included in this thesis (section 6).

Glossary

AP Action potential

APD Action potential duration

ATP Adenosine triphosphate

β-AR β-adrenergic receptor

Ca^{2+} Calcium ion

CaM Calmodulin

CaMKII Calmodulin kinase II

CICR Calcium-induced calcium release

EAD Early after-depolarization

EC coupling Excitation-Contraction coupling

JSR Junctional Sarcoplasmic Reticulum

K^+ Potassium ion

LCC L-type calcium channel

Mg^{2+} Magnesium ion

Na^+ Sodium ion

NSR Network Sarcoplasmic Reticulum

PKA Protein kinase A

SERCA Sarco(endo)plasmic reticulum Ca-ATPase

SR Sarcoplasmic reticulum

RyR Cardiac isoform of ryanodine receptor

Chapter 2

Background on cardiobiology

2.1 The heart

The heart is a four-chambered electromechanical device, whose task is to pump blood. It consists of two pumps in series: the right atrium and ventricle to propel blood through the lungs for exchange of oxygen and carbon dioxide (the pulmonary circulation) and the left atrium and ventricle to propel blood to all other tissues of the body (the systemic circulation).

Contractions of the heart are driven by an electrical impulse called the action potential (AP) which conducts throughout the heart muscle through the cardiac conduction system. On each heartbeat, electrical excitation originates in a specialized pacemaker region known as the sinoatrial node. The activity spreads through the upper chambers of the heart (the atria), then through the atrioventricular node and the His-Purkinje system to the lower chambers of the heart (the ventricles), inducing contraction of each chamber. Abnormalities, such as blocks and loops in conduction pathways, lead to cardiac diseases [48]. In summary, an action potential traveling in the heart muscle triggers contraction of individual myocytes and thereby contraction of the heart.

2.2 Cardiac action potential and ion channels

Regulating the internal composition of myoplasm is a key process in maintaining the chemistry of life, two of the most fundamental components of which are concentration and intracellular/extracellular balance of biologically important ions, including sodium (Na^+), potassium (K^+), and calcium (Ca^{2+}). Since the phospholipid membrane is almost totally impermeable to ions, there is a need for ion channels to transport ions in and out of the cell

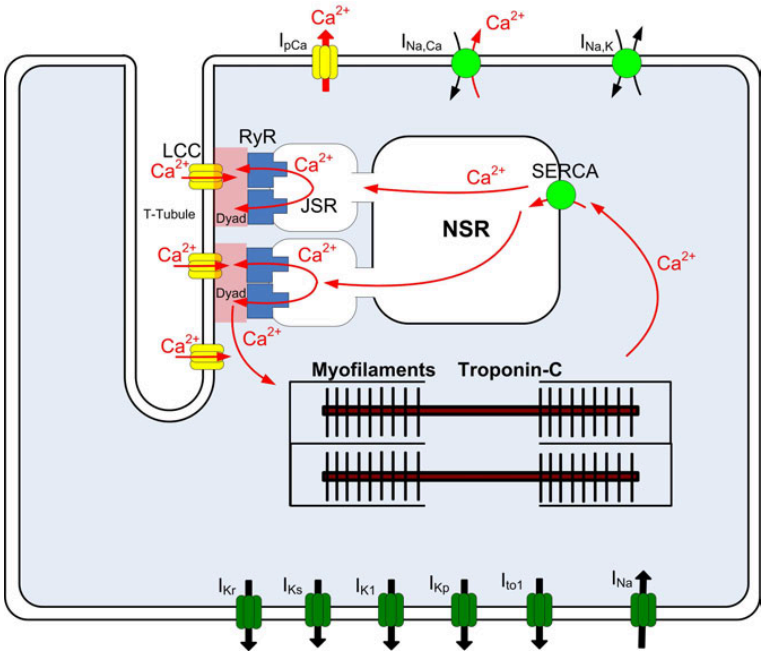

Figure 2.1: A cartoon showing Ca^{2+} cycling and the major ionic currents present in a cardiac myocyte (channel terminology as in Greenstein et al. [34]). Briefly, in response to membrane depolarization Ca^{2+} enters the cell through LCCs from T-tubules, which triggers further Ca^{2+} release from the Junctional Sarcoplasmic Reticulum (JSR). This leads to an increase in myoplasmic Ca^{2+} concentration, to the binding of Ca^{2+} ions to Tropinin-C, activation of myofilaments, and to the consequent contraction of the myocyte. After detaching from myofilaments, Ca^{2+} ions are mostly either sequestered to the Network Sarcoplasmic Reticulum (NSR) by the Sarco(endo)plasmic reticulum Ca-ATPase (SERCA) or extruded by sodium calcium exchanger ($I_{\mathrm{Na,Ca}}$).

through the membrane. Propagation of cardiac action potential depends on ion channels (Fig. 2.1), and it reflects activity of over 20 ion channel types [68] out of the total of 400 known ion channel types [29].

At the cellular level, the AP is associated with cyclic changes in the electrical potential difference across the cell membrane known as membrane potential (Fig. 2.2). The membrane potential is changed by ions flowing through ion channels. During resting conditions (diastole), cell membrane is highly permeable to K^+ ions, but almost totally impermeable to Na^+ ions. Membrane potential of a myocyte is approximately -90 mV during diastole.

Electrical excitability of myocytes is mainly due to an imbalance of Na^+ and K^+ between extracellular space and myoplasm. At the beginning of an AP (phase 0), a small electrical signal (stimulus) triggers opening of Na^+ channels which results in a large and very brief influx of Na^+ ions and thereby a rapid depolarization of the myocyte (phase 1 in Fig. 2.2). Membrane potential first hits 0 mV, and then overshoots to about $+40$ mV. This results opening of ion channels responsible for the transient outward current (membrane current I_{to1}), which rapidly depolarizes the cell (notch after phase 1 in Fig. 2.2). This enables opening of Ca^{2+} channels allowing influx of Ca^{2+} ($I_{\mathrm{Ca,L}}$) necessary for the initiation of contraction. After the "notch" in AP, inward K^+ currents (I_{Kr} and I_{Ks}) slowly repolarize the cell during the plateau phase (phase 2). After the plateau phase, rectifying K^+ currents (mainly I_{K1}) and inactivation of $I_{\mathrm{Ca,L}}$ rapidly repolarize the cell (phase 3) to diastolic membrane potential (phase 4). Thus, the changes in membrane potential lead to a sequence of events that result in the contraction of the heart muscle and the consequent pumping of blood through the body.

The AP of ventricular myocytes is characterized by a long plateau phase (Fig. 2.2), during which many events are triggered that initiate and control mechanical contraction. The long plateau is also necessary to keep the myocyte from responding to a secondary excitation known as early afterdepolarization.

2.3 Excitation-Contraction coupling

Translation of electrical excitation (the AP) to contraction of the heart is known as Excitation-Contraction (EC) coupling. Contraction of the cardiac myocytes occurs only after individual L-type calcium channels (LCCs, see Bers[10]; $I_{\mathrm{Ca,L}}$ flows through LCCs) open in response to membrane depolarization producing Ca^{2+} flux into a small microdomain known as the cardiac dyad[1] [10]. The resulting influx of Ca^{2+} ions leads to opening of RyRs located

[1] Term 'diad' is also commonly used to refer to the same domain.

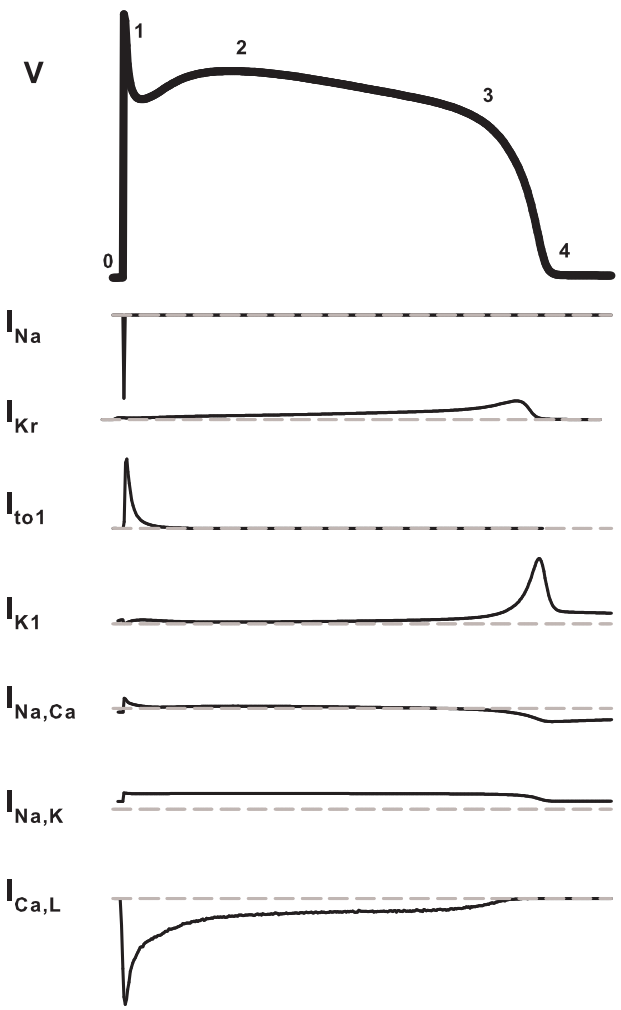

Figure 2.2: Ventricular action potential (top) with numbers 0-4 referring to the phase of the AP, simulated with the Greenstein-Winslow model [34]. Phase 2 is the plateau phase. The major ionic membrane currents (not in scale) operating during an AP: I_{Na}, cardiac sodium current; I_{Kr}, rapid component of the delayed rectifier current; I_{to1}, cardiac transient outward current 1; I_{K1}, inwardly rectified potassium current; $I_{\mathrm{Na,Ca}}$, cardiac sodium calcium exchanger; $I_{\mathrm{Na,K}}$, cardiac sodium potassium ATPase; and $I_{\mathrm{Ca,L}}$, cardiac L-type calcium current.

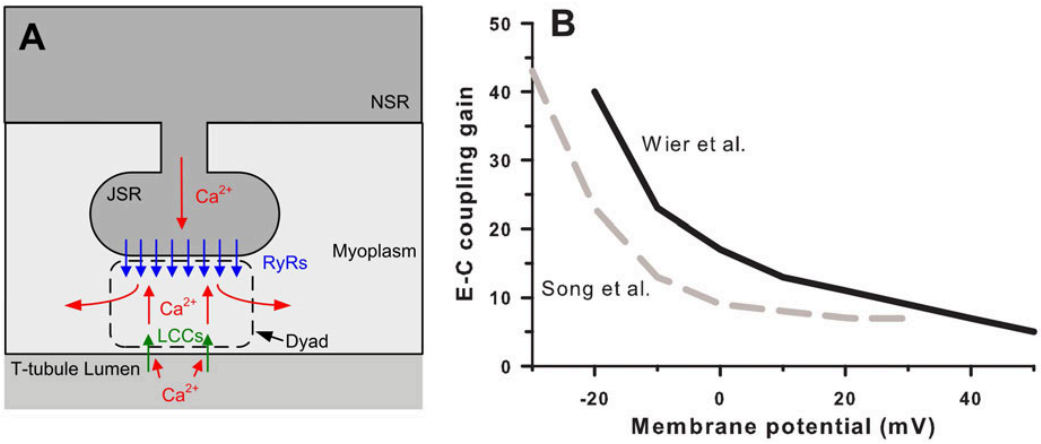

Figure 2.3: CICR in the cardiac dyad: (A) In response to membrane depolarization, LCCs open and allow Ca^{2+} to enter the cardiac dyad from the T-tubule lumen. These Ca^{2+} ions bind to RyRs and thereby trigger opening of RyRs, which enables Ca^{2+} release from the JSR. (B) EC coupling gain (defined as the ratio of peak Ca^{2+} flux through RyRs to peak Ca^{2+} flux through LCCs) measured in experimental studies of Wier et al. [103] and in Song et al. [83] is a decreasing function of clamp voltage.

in the closely apposed Junctional Sarcoplasmic Reticulum (JSR) membrane and to additional flux of Ca^{2+} ions from the JSR into the dyad (Fig. 2.3A). This process is known as calcium-induced calcium release (CICR) [10], and it was first proposed by Endo [26] as a mechanism for EC coupling in skeletal muscle. These two sources (RyRs and LCCs) of Ca^{2+} flux produce the intracellular Ca^{2+} transient leading to binding of Ca^{2+} ions to Troponin-C, activation of myofilaments, and ultimately to the cardiac muscle contraction (Fig. 2.1). Thus, Ca^{2+} acts as a second messenger in EC coupling.

The cardiac dyad is a small space between the sarcolemma and Sarcoplasmic reticulum (SR; consists of JSR and NSR) in which CICR takes place. The dyad is often approximated as a cylinder of height of 15 nm and radius of 100-400 nm (Figures 2.1 and 2.3A; for more details see, e.g., Bers [10]) or as a box of similar magnitude. The dyad contains 20-100 RyRs and 5-20 LCCs, typically in ratio 1:5 of LCCs to RyRs [10].

Most ($> 95\%$) of the Ca^{2+} released to myoplasm is buffered by Ca^{2+} buffers[10]. While most of Ca^{2+} buffering is by immobile Ca^{2+} buffers, Ca^{2+} is also buffered by mobile Ca^{2+} buffers (mainly ATP and CaM). Only a small fraction of all Ca^{2+} is free in myoplasm.

The majority of Ca^{2+} entering the myoplasm during EC coupling is re-

leased from the SR, only a fraction enters the cell through the LCCs [103]. The rate and magnitude of Ca^{2+} release from the SR is tightly controlled by the magnitude and duration of L-type Ca^{2+} current.

The relative magnitude of Ca^{2+} fluxes through LCCs and RyRs is measured by EC coupling gain defined as the ratio of peak Ca^{2+} flux through RyRs and peak Ca^{2+} flux through LCCs (Fig. 2.3B). EC coupling gain is measured experimentally in a voltage-clamp protocol typically with 10 mV, 100 ms steps from -40 mV to +50 mV from a holding potential of -100 mV. While peak Ca^{2+} fluxes through both LCCs and RyRs have bell shapes as a function of voltage in this protocol, EC coupling gain typically has a decreasing shape (Fig. 2.3B) as a result of a shift between peak LCC and RyR fluxes [10, 103]. The presence of this shift strongly suggests that EC coupling gain depends on local dyadic Ca^{2+} concentration [85].

The decreasing shape of EC coupling gain is a result of combination of the driving force of Ca^{2+} flux through LCCs and open probabilities of LCCs at various voltages, which together determine the local dyadic Ca^{2+} trigger driving the opening of RyRs. At a polarized (e.g., -40 mV) voltage, the driving force of Ca^{2+} influx is high (for details, see Sec. 3.1), however, only relatively few L-type Ca^{2+} channels open, which results high local Ca^{2+} concentrations in a few cardiac dyads. Opening of RyRs depends on the dyadic Ca^{2+} concentration, and a high dyadic Ca^{2+} concentration is converted to a high opening probability of RyRs, which results high EC coupling gain. At a higher, more depolarized voltage, driving force is low but many L-type Ca^{2+} channels open which results in low Ca^{2+} concentrations in many dyads. Thus, only a few RyRs open and the resulting EC coupling gain is low.

To make CICR a robust process, Ca^{2+} release must stop at some point. To ensure this, LCCs exhibit two separate inactivation processes: Ca^{2+}-dependent inactivation and voltage-inactivation. Similarly, RyRs exhibit Ca^{2+}-dependent inactivation, but also other mechanisms such as RyRs regulation by luminal Ca^{2+}, and allosteric interactions between neighboring RyRs, which all assist in extinguishing Ca^{2+} sparks (for more details, see Bers [10]). The details of these mechanisms and their relative importance are under vigorous investigation.

CICR provides a prime example of the presence of shot noise in a cellular process. Even at peak, only 1-100 free Ca^{2+} ions are present in the dyad [10], which suggests that noise due to the discreteness of Ca^{2+} ions may have a significant influence on CICR. The influence of this noise source on EC coupling has not previously been studied, but it is examined in article III. Since CICR is central to EC coupling in the heart, understanding the molecular basis of CICR is of fundamental importance to understanding cardiac muscle function in both health and disease.

Chapter 3

Mathematical models of excitable cells

Cardiac myocytes belong to the class of excitable systems that includes, e.g., neural cells, magnetospheric substorms, and lasers. While excitable systems operate in a wide variety of environments, excitable systems share a number of general characteristics [55]. One of the main characteristics is the presence of non-linear positive feedback, that is, a small signal may trigger a large response. In a cardiac myocyte, this is evidenced by the rapid depolarization in response to a stimulus. Following a stimulus, a cardiac myocyte has a refractory period during which a second excitation is not possible. A refractory period is also present in most excitable systems. To list one more characteristic, an excitable system is also typically far from being at thermodynamic equilibrium. For example, a myocyte is kept excitable in a non-equilibrium state by K^+ and Na^+ electrochemical gradients between intracellular and extracellular spaces maintained by ion pumps and exchangers [38].

In electrophysiological cell modeling, the objects of interest are typically the action potential, ionic and molecular concentrations, and fluxes associated with them. Most computational cell models are based on a set of ordinary differential equations, in which the number of equations is within range one to a hundred. The first electrophysiological model of a heart cell was the Van der Pol-oscillator [92]. While Van der Pol-oscillator is not really a model of an excitable cell nor can it be considered a biophysically detailed model due to the lack of ionic currents in the model, it has spawned a large variety of models of excitable cells found in the scientific literature today, a few of which are described in the following sections.

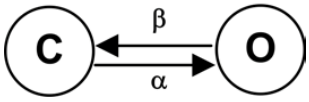

Figure 3.1: Gating scheme of a single Hodgkin-Huxley gate [41]. Transition rates between open (O) and closed (C) states are given by α and β.

3.1 Hodgkin-Huxley model of the neural AP

The first biophysically detailed mathematical model of the neural AP was formulated by Hodgkin and Huxley [41], who investigated giant squid axons. In the Hodgkin-Huxley model, membrane potential V is driven by three membrane currents: potassium current I_{K}, sodium current I_{Na}, and leak current I_{L}. In more mathematical terms, voltage evolves according to

$$dV(t)/dt = -(I_{\mathrm{Na}} + I_{\mathrm{K}} + I_{\mathrm{L}})/C_m, \quad V(0) = V_0, \tag{3.1}$$

where $t \in \mathbb{R}$ is time, $V : \mathbb{R} \to \mathbb{R}$ is membrane potential, V_0 is the initial membrane potential, and $C_m \in \mathbb{R}$ is (specific) membrane capacitance. The minus sign in equation (3.1) is a convention stating that an inward current has a negative sign and an outward current has a positive sign.

Membrane current I_k, where $k \in \{\mathrm{Na}^+, \mathrm{K}^+, \mathrm{L}\}$, was in Hodgkin-Huxley model defined by

$$I_k(t, V) = g_k(V - E_k)[a_k(t, V)]^{n_k}[b_k(t, V)]^{m_k}, \tag{3.2}$$

which depends on reversal potential $E_k \in \mathbb{R}$ (depending on intracellular and extracellular ionic concentrations), membrane potential V, and the maximal total membrane conductance $g_k \in \mathbb{R}$ of current k. Difference $V - E_k$ is called the *driving force*, and it largely determines the magnitude and direction of ionic current k.

In the Hodgkin-Huxley model[1], membrane currents depend on 2-state gates that can be open or closed (Fig. 3.1). The ion channels conduct only when the activating gates are open and the inactivating gates are closed. In equation (3.2), the ratio of activating gates in open state is described by gating variable $a_k : \mathbb{R}^2 \to [0, 1]$ and the ratio of inactivating gates in closed state is described by gating variable $b_k : \mathbb{R}^2 \to [0, 1]$. Constants $m_k, n_k \in \mathbb{N}$

[1]During the 1950s when the Hodgkin-Huxley model [41] was formulated, there was no knowledge of ion channels. Nevertheless, Hodgkin and Huxley made the bold hypothesis that such machines exist, and proceeded to formulate a revolutionary model of the nerve cells.

defined the number of activating and inactivating gates associated with each ion channel, respectively.

The rate at which ion channels open and close is different for each channel type, and it is largely based on the potential difference (membrane potential) across the membrane in which they are embedded. Of the three currents, I_{L} gated independently of voltage (thus, $a_L = b_L = 1$), while gating of I_{Na} and I_{K} depended on membrane potential. Gating variables $a_k, b_k : \mathbb{R}^2 \to \mathbb{R}$ for $k \in \{\mathrm{Na}^+, \mathrm{K}^+\}$ evolved according to

$$da_k(t,V)/dt = \alpha_k(V)(1 - a_k(t,V)) - \beta_k(V)a_k(t,V),\ a_k(0,V_0) = a_{k,0}, \quad (3.3)$$
$$db_k(t,V)/dt = \alpha'_k(V)(1 - b_k(t,V)) - \beta'_k(V)b_k(t,V),\ b_k(0,V_0) = b_{k,0}, \quad (3.4)$$

where rates $\alpha_k, \alpha'_k, \beta_k, \beta'_k : \mathbb{R} \to \mathbb{R}$ depend on voltage V, and initial values of gating variables are given by $a_{k,0}, b_{k,0} \in \mathbb{R}$. To complete the model definition, rates α_k and β_k must be found experimentally, e.g., rates

$$\alpha_{\mathrm{Na}^+}(V) = 0.1(V + 25)/(e^{0.1(V+25)} - 1), \quad (3.5)$$
$$\beta_{\mathrm{Na}^+}(V) = 4e^{V/18} \quad (3.6)$$

defined the transition rates of activating gates associated with I_{Na} in the Hodgkin-Huxley model [41].

The Hodgkin-Huxley model employed the mean-field approximation, that is, gating variables described the expected ratio of gates in one of the allowed states. Use of mean-field approximation is reasonable, since an axon contains 125 Na^+ [5] channels and 30 K^+ channels per $\mu\mathrm{m}^2$ membrane area, which yields $1,250,000$ Na^+ and $300,000$ K^+ channels per axon (assuming membrane area of $10^4\mu\mathrm{m}^2$) [19]. The Hodgkin-Huxley model assumed that ionic concentrations are unchanged during the simulation period, which restricts the model to describe short-term behavior of an axon.

While the Hodgkin-Huxley model defined by equations (3.1)-(3.6) looks deceptively simple, it nevertheless captures a significant amount of electrophysiology of neural cells. These considerations together with experimental advances brought a Nobel prize to Hodgkin and Huxley in 1963 for "their discoveries concerning the ionic mechanisms involved in excitation and inhibition in the peripheral and central portions of the nerve cell membrane". More than 50 years after the discoveries of Hodgkin and Huxley, simple neural models still offer surprises, in particular when gating noise is incorporated in such a model [102].

3.2 Models of a cardiac myocyte

Similarly to axons considered by Hodgkin and Huxley [41], cardiac myocytes are excitable cells. Consequently, a model of the cardiac AP similar to the Hodgkin and Huxley model [41] was subsequently derived by Beeler and Reuter [8].

DiFrancesco and Noble [24] developed a more realistic electrophysiological model of an isolated ventricular myocyte that in addition to ion channels described similarly to those in the Hodgkin-Huxley model [41], also included models for Na-K pump, Na-Ca exchanger, the SERCA pump, and dynamically evolving ionic concentrations. The DiFrancesco and Noble model [24] demonstrated that electrophysiological properties and processes of a cardiac cells can be elucidated using a mathematical model, e.g., the model successfully reproduced intracellular sodium concentration changes produced by variations in extracellular sodium or by Na-K pump block. The DiFrancesco-Noble model [24] has subsequently served as a basis for more recent integrative models of a cardiac myocyte.

The most influential integrative models of ventricular myocytes today are likely those of Luo and Rudy [56, 57, 58], Noble et al. [67], and Winslow et al. [106], and their subsequent refinements. The phase II Luo-Rudy [57] model provided a detailed multicompartment model of AP in guinea pig ventricular myocytes, and it also described most of the membrane currents present in a ventricular myocyte. The phase II Luo-Rudy model [57] is still often taken as a starting point of more refined modeling. While Luo and Rudy [57] investigated Ca^{2+} dynamics in a ventricular myocyte, their model did not contain a detailed model of dyadic Ca^{2+} dynamics.

One of the most important issues in the electrophysiological modeling of a cardiac myocyte is realistic description of CICR, which requires a detailed model of Ca^{2+} dynamics in the cardiac dyad. The canine AP model of Winslow et al. [106] represented a left ventricular myocyte as a set of interconnected compartments with the cardiac dyad as one of the compartments. A major improvement in the model of Winslow et al. [106] over the previous myocyte models was a more realistic modeling of CICR, and a 'minimal' reproduction of the heart failure phenotype in a cardiac myocyte. Subsequent refinements of the Winslow et al. model [106] have improved CICR modeling [34, 32].

Development of computational models of cardiac cells is an active area of research, as is shown by the large number of models of cardiac myocytes presented recently, e.g., [47, 91, 79, 20]. Nevertheless, most integrative models of a cardiac myocyte are still based on the paradigm developed by Hodgkin and Huxley and refined by DiFrancesco and Noble [24].

3.2.1 A schematic model of a cardiac myocyte

To make things more concrete, the following equations define a schematic electrophysiological single-compartment model of the AP in cardiac myocyte:

$$dV/dt = -\sum_q \sum_{r \in S_q} I_r/C_m - I_{\text{stim}}/C_m,\ V(0) = V_0, \tag{3.7}$$

$$dc_q/dt = -\sum_{r \in S_q} I_r/z_q F v,\ c_q(0) = c_{q,0}, \quad \text{where } q \in \{\text{Na}^+, \text{Ca}^{2+}\}, \tag{3.8}$$

$$dc_{\text{K}^+}/dt = -\sum_{r \in S_{\text{K}^+}} I_r/Fv - I_{\text{stim}}/Fv,\ c_{\text{K}^+}(0) = c_{\text{K}^+,0} \tag{3.9}$$

$$I_k(t, V) = g_k D_k(V, c_{q_1}, c_{q_2}) P_{k,O}(t, V), \tag{3.10}$$

where k indexes the set M of membrane currents due to ion channels, $q_k \in \{\text{K}^+, \text{Na}^+, \text{Ca}^{2+}\}$, S_n is the set of membrane currents carrying ion species $n \in \{\text{K}^+, \text{Na}^+, \text{Ca}^{2+}\}$, z_q is valence of ion species q, F is the Faraday constant, and v is the volume of myoplasm. Extracellular ion concentrations c_q^o are assumed to be constant. Initial values of the variables are given by $V_0, c_{q,0} \in \mathbb{R}$.

Equation (3.7) states that time-evolution of membrane potential V depends on all ionic membrane currents, including the stimulus current I_{stim} used to induce the AP in a myocyte[2]. Equation (3.8) defines the time-evolution of ionic concentrations c_{Na^+} and $c_{\text{Ca}^{2+}}$, while equation (3.9) defines the time-evolution of c_{K^+} ion concentrations, since the stimulus current is assigned to c_{K^+}, that is, to potassium concentration.

Membrane currents are defined by equation (3.10), where g_k is the maximal conductance of current k. Function $D_k : \mathbb{R}^3 \to \mathbb{R}$ describes the driving force of membrane current k, e.g., $D_k(v, c_q, \cdot) = v - RT \ln(c_q^0/c_q)/z_q F$ was chosen in the Hodgkin-Huxley model [41], where term $RT \ln(c_q^0/c_q)/z_q F$ is the reversal potential of ion species q, R is the universal gas constant, and T is the absolute temperature. More generally, membrane current due to an exchanger or a cotransporter depends on intracellular ion concentrations c_{q_1}, c_{q_2} and on extracellular ion concentrations $c_{q_1}^o, c_{q_2}^o$ of ion species q_1 and q_2. The actual membrane current then consists of two components, one for each ion species. Hence, the driving force depends on concentrations of two ion species. The two currents are treated separately in this formulation.

In modern integrative cell models, Hodgkin-Huxley type gating schemes are often replaced by more detailed Markov processes.Assuming the kinetics of an ion channel are described by a discrete-state, continuous-time Markov

[2]Stimulus current I_{stim} is a time-dependent current, the exact shape and time-dependence of which depends on the experimental protocol used.

process, probability $P_{k,s}$ of state $s \in \Omega_k$ of membrane current k evolves according to equation

$$dP_{k,s}(t,V)/dt = \sum_{u \neq s} (\alpha_{su}^{(k)}(V) P_{k,u}(t,V) - \alpha_{us}^{(k)}(V) P_{k,u}(t,V)), \tag{3.11}$$

where $P_{k,s}(0,V_0) = P_{k,s,0} \in \mathbb{R}$ gives the initial value, Ω_k is the set of states of the Markov process describing ion channel kinetics associated with current k. Transition rate in the Markov model from state u to state s are described by $\alpha_{su}^{(k)}$. For voltage-gated ion channels, rates $\alpha_{ab}^{(k)}$ depend on voltage V, but for ligand-gated ion channels rates also depend on ligand concentrations.

Combining equations (3.7)-(3.9), and then integrating shows that the set of equations describes a capacitor. This requires that all membrane currents crossing the cell membrane influence membrane potential and must hence be included in equation (3.7) and in one of the concentration equation[3]. In the above-defined model, the stimulus current is assigned to myoplasmic potassium concentration, c_{K^+}. Hence, set (3.7)-(3.11) of equations is overdetermined and equations (3.8)-(3.11) suffice to define the model, since voltage is a function of ionic concentrations.

The Poincare-Bendixson theorem (e.g., [89]) states that if an orbit of a continuous two-dimensional dynamical system stays in a bounded region of the state space, it either approaches a fixed point or possesses a limit cycle. For a higher-dimensional dynamical systems, this is not necessarily true, and chaos may be present [28]. In a model of the cardiac AP stimulated periodically, a stimulation rate-dependent limit cycle typically exists given physiologically-relevant parameters and initial conditions, even if relatively small parameter changes may push the system to a bifurcation regime or even to a chaotic regime.

The Winslow et al. model [106] consisted of a set of 31 ordinary differential equations. While the model is stable (that is, the model has a limit cycle) under regular conditions, a bifurcation point emerges when myoplasmic Na^+ concentration increases significantly beyond 12 mmol/L (the exact value depends on various parameter settings), and the model shows cardiac alternan-like behavior. This demonstrates that a high-dimensional dynamical model does not necessarily have a well-defined limit cycle under realistic physiological conditions. Given that a significant noise component is present in experimentally measured membrane currents, interplay between stochastic and deterministic "chaos-theoretic" components may be important near bifurcation points, which is not captured by mean-field models such as the Winslow et al. model [106].

[3]This has not been the case in all integrative models described in the literature. Hence, not all integrative models have been charge-conservative. For details, see [93, 43, 35, 90].

The main difference of a model based on equations (3.8)-(3.11) to the Hodgkin-Huxley model (equations (3.1)-(3.6)) is that ionic concentrations are dynamical (equations (3.8) and (3.9)), and that more general ion channel gating and conduction models are used. The schematic setting defined by equations (3.8)-(3.11) can be found in most modern integrative myocyte models.

3.3 Markov models of ion channel gating

Gating of ion channels is in central role in an electrophysiological cell model. In a Hodgkin-Huxley type model, ion channel gating (equations (3.2)-(3.4)) consist of on-off switches, which can be interpreted as 2-state continuous-time Markov processes. More specifically, a stochastic process X defined on a complete filtered probability space $(\Omega, P, \{F_t\}, \mathcal{F})$ is a continuous-time, finite-state Markov process if

$$P(X(t+s) \leq a | X(s) = x, X(u), 0 \leq u < s) = P(X(t+s) \leq a | X(s) = x), \tag{3.12}$$

for all $t, s \in \mathbb{R}, s \geq 0$, and its state space Ω is finite (above $x \in \Omega$). Markov processes are memoryless stochastic processes, and they provide a natural framework[4] for generalizing Hodgkin-Huxley gating schemes (e.g., Winslow et al. [106]). Unlike in more common applications of Markov processes, in Markov process-based models (Markov models in the following) describing ion channel gating, transition rates depend on membrane potential (as in equations (3.5)-(3.6)), or on ligand concentrations.

Several Markov models can be combined to a single compound model (Fig. 3.2). Counterintuitively, a compound model may reduce the complexity of a cell model, since it may enable the use of the steady state approximation for ion concentrations separately for each state of the compound model of ion channels (e.g., Hinch et al. [39]).

Ion channels are molecular machines that operate according to the laws of statistical mechanics. Hence, to ensure that the second law of thermodynamics is not violated, a Markov model describing ion channel gating should be reversible, which corresponds to concepts of microscopic reversibility and detailed balance in statistical physics. This ensures that no energetically-free cycling is present in thermodynamic equilibrium.

Estimating parameters of a model is of fundamental importance in modeling experimental measurements. A variety of methods have been employed

[4] In this thesis, gating kinetics schemes are based on continuous-time finite-state Markov processes. While infinite-state Markov processes have been used to describe gating kinetics (e.g., Hänggi et al. [31]), their impact on integrative models has been limited.

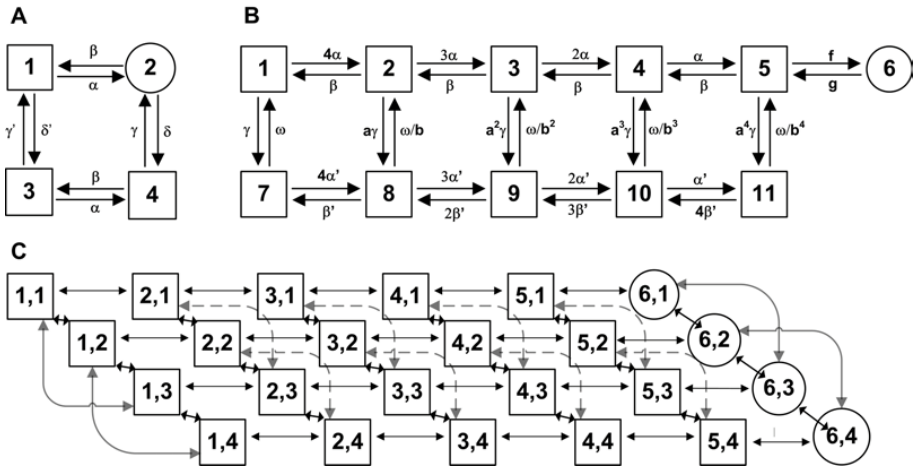

Figure 3.2: Markov model of (A) RyR, in which state number 2 is the only open state; and (B) LCC in which the top row is high-activity 'Mode Normal' (non-Ca^{2+}-inactivated state of the ion channel) and lower row is low-activity 'Mode Ca' (Ca^{2+}-inactivated state) [110, 106]. State number 6 is the open state of the channel. Direct product of the RyR and LCC models yields (C) a compound model consisting of two layers of which only 'Mode Normal' is shown.

in the literature to fit parameters to Markov models of ion channels, including the Ordinary least squares method (e.g., Iyer et al. [47]), Maximum likelihood (e.g., Saftenku et al. [77]), Bayesian methods (e.g., Hodgson [42]), and inverse methods (e.g., Cannon and D'Alessandro [15]).

The myocyte models presented in this thesis were mostly fitted using the Ordinary least squares method, in which fitting is accomplished by minimizing a sum-squared error function generated by comparing the forecasted currents (obtained from equation (3.14)) to goal data typically obtained in voltage-clamp protocols [47]. The two main methods to extract information from a Markov model describing ion channel gating are (1) mean-field approximation; and (2) stochastic single channel simulation.

3.3.1 Mean-field approximation

Vector-valued function $P : \mathbb{R}^2 \to \mathbb{R}^n$ describing the probability of each state of a continuous-time Markov process (Markov model) at time t evolves as

$$\frac{dP(t, V_t)}{dt} = A(V_t)P(t, V_t), \tag{3.13}$$

where matrix-valued function $A : \mathbb{R} \to \mathbb{R}^{n \times n}$ describes membrane potential (denoted here by V_t) dependent transition rates of the Markov process. This approach can be interpreted as a mean-field approximation, since given the number of ion channels, denoted here by N, the average number of channels in state k is NP_k.

Under conditions of applied voltage clamp (that is, constant V_t), differential equation (3.13) can be written as a linear time-invariant system. The solution of this system is thus a weighted sum of exponentials (assuming that eigenvectors $\{e_k\}_k$ are linearly independent)

$$P(t) = \sum_k w_k e_k e^{\lambda_k t}, \tag{3.14}$$

where $\lambda_k \in \mathbb{R}$ is the kth eigenvalue of matrix $A(V_t)$, $e_k \in \mathbb{R}^n$ is its corresponding eigenvector, and weights $w_k \in \mathbb{R}$ are constants of integration determined by the initial value vector $P(0)$.

3.3.2 Stochastic simulation

Voltage-gated ion channels are devices operating in a stochastic manner [61]: a large ensemble of ion channels gate in a rather orderly fashion, but individual ion channels gate in a stochastic fashion. In a stochastic simulation,

each channel can be described as a single entity, each of which is represented as a Markov process.

One of the most efficient methods to simulate a continuous-time Markov process is the exact method of Gillespie [30, 13] in which time-step to the next state transition is given by $\tau = \log(r)/k$, where r is a uniformly in $(0, 1)$ distributed random number and k is the sum of exit rates from the current state of the Markov process. If multiple exit rates are available, the one occurring is chosen according to the corresponding ratio of transition rate to the total transition rate.

When the number of ion channels is large, it suffices for many purposes to consider average properties of an ion channel ensemble using the mean field approach (equation (3.13)). However, when the number of ion channels is small, gating noise due to fluctuations in the number of open channels will have a large impact on the results, and stochastic simulation is the only way to proceed.

3.4 Modeling cardiac diseases computational *in silico*

Proper functioning of ion channels is crucial to human physiology as is demonstrated by, e.g., the recent finding that an inheritable mutation in a gene encoding a single type of sodium channel is sufficient to completely remove the sense of pain [22]. Hence it is not surprising that disorders of ion channels make up a key group of heart diseases, because the heart beat is so dependent on the proper movement of ions across the surface membranes [59].

Linking molecular defects in ion channels to integrated function of an organ is not an easy task. Experiments alone are not sufficient to provide complete understanding of the heart and its disorders. However, coupling of experimental results to computational models has enabled *in silico* examination of disorders in the heart [44], which has brought significant elucidation of the processes of the heart [63]. This was shown by, e.g., Winslow et al. [106] who investigated quantitatively the impact of the expression level of the gene encoding the SERCA pump on APD and Ca^{2+} homeostasis in a cardiac ventricular myocyte. Winslow et al. [106] also reconstructed the heart failure phenotype of a cardiac myocyte based on experimentally observed expression levels of a gene encoding SERCA pump, sodium-calcium exchanger, and changes in potassium and certain other ionic currents under heart failure condition (Fig. 3.3). In these experiments, myocytes characterized as failing

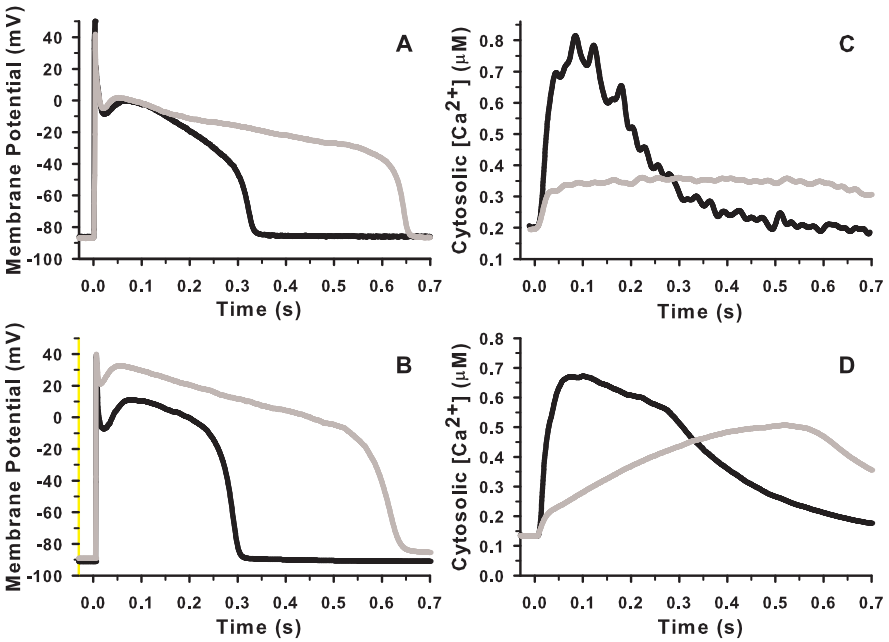

Figure 3.3: Comparison of experimental measurements on normal and failing canine cardiac myocytes with the computational reproduction of experimental measurements using the model of Winslow et al. [106]: (A) Experimentally measured AP in a normal (black line) and a failing myocyte (light grey line); (B) Computationally reproduced AP in a normal (black line) and a failing myocyte (light grey line); (C) Experimentally measured myoplasmic Ca^{2+} transients in a normal (black line) and a failing myocyte (light grey line); (D) Computationally reproduced myoplasmic Ca^{2+} transients in a normal (black line) and a failing myocyte (light grey line).

were isolated from canine hearts subjected to the tachycardia pacing protocol [71].

An arrhythmia is a disturbance of the cardiac rhythm, which may lead to severe or even fatal complications [59, 64]. Over 40 drugs are available to treat various heart conditions, with cardiac arrhythmia representing a significant segment of the drug market [68]. Understanding the electrophysiology of the heart is also critical to resolving a major problem for the drug industry: a large number of compounds target the proteins involved in cardiac repolarization, so causing arrhythmia can be fatal [64]. Painkiller rofecoxib, marketed as Vioxx, is a prime example of the issues: it was on the market for five years before it was found to increase the risk of heart attacks and strokes in long-term users [21]. This necessitates computational investigation of, e.g., the possible cellular triggers of arrytmias [64, 105].

A clear understanding of how cellular and molecular processes regulate Ca^{2+} movements should help make it possible to design novel drugs that act specifically at strategic locations in the heart. Biophysically detailed models have significantly contributed to our understanding of processes influencing action potential shape and duration in normal myocytes[105]. As a further development, electrophysiological models have also been applied to investigation of genetic and molecular basis of arrhythmia. In more detail, models have been applied to investigate EADs [113, 97], mechanisms of delayed after-depolarizations [95, 94], consequences of gene mutations [17], and altered gene expression at the cellular level [106]. The results of these studies demonstrate that modeling can significant advance our understanding of the heart in both health and disease, which is a prerequisite of the development of more efficient and safe drugs.

In summary, cardiac myocytes have been extensively studied, and it has been claimed that "if there is a virtual cell to be had, it is cardiac myocyte" [105]. Nevertheless, significant gaps persist in our knowledge of the details of the cardiac myocyte function. An example of such a gap is how Ca^{2+} sparks are extinguished, that is, how RyRs close at the end of a Ca^{2+} release event in the cardiac dyad [86].

Chapter 4

Models of CICR in the cardiac dyad

A recurrent theme in biology is the modeling of small microdomains controlling significantly larger processes. An example of this is CICR taking place in the cardiac dyad, which controls the amount of free myoplasmic Ca^{2+} in a cardiac myocyte and thereby determines the strength of the heart contraction. Since EC coupling depends on CICR, detailed description of the dyadic Ca^{2+} dynamics is a central issue in computational cardiobiology.

4.1 Integrative models and the cardiac dyad

An integrative computational model of a myocyte enables investigation of the interrelationship between microscopic and macroscopic cellular processes that would not be possible in experiments. To enable realistic *in silico* experiments, an integrative model of a cardiac myocyte must describe physiological processes relevant for the investigation. For example, to investigate the connection of macroscopic EC coupling to the underlying microscopic events, CICR occurring in the cardiac dyad must be modeled in detail.

A number of integrative models of the cardiac myocyte have been proposed in the literature, e.g., [24, 57, 67, 106]. The first integrative models explicitly containing the cardiac dyad were the canine AP model of Winslow et al. [106] and the guinea pig AP model of Noble et al. [67]. In the model of Winslow et al. [106], a cardiac myocyte was divided into four compartments: myoplasm, NSR, JSR, and the cardiac dyad. Ca^{2+} release from the RyRs depended on dyadic Ca^{2+} concentration, that is, CICR took place in the cardiac dyad. While the Winslow et al. model [106] reproduced a large amount of experimental data, it assumed that *all* RyRs in the myocyte observe identical

dyadic Ca^{2+} concentration, and that both the trigger Ca^{2+} and the released Ca^{2+} pass through a common pool during CICR. This approach is known as the *common pool* approach [85]. Similarly, Ca^{2+} passed through a common pool during CICR in the model of Noble et al. [67], which is also a common pool model[1].

It has been known for over 35 years that contraction amplitude of a cardiac myocyte is a smoothly graded function of membrane potential during voltage clamp depolarization [62, 85]. In a common pool model, Ca^{2+} release is always triggered when Ca^{2+} concentration in the common dyadic pool crosses a threshold. Hence, in a common pool model, Ca^{2+} release is necessarily of all-or-none type, and not a graded function of voltage-clamp potential, as found in experimental studies [103, 62]. Stern [85] showed that a common pool model cannot produce both high EC coupling gain and graded Ca^{2+} release, if magnitudes of Ca^{2+} fluxes are physically relevant. Since physiological role of CICR is to provide high amplification of trigger Ca^{2+}, inability to reproduce both the high gain and graded release is a significant issue for an integrative model.

Stern [85] introduced models based on the *local control* hypothesis, in which gating of RyRs and LCCs depend on local Ca^{2+} concentration in the cardiac dyad, not on Ca^{2+} concentration in any pool common to all LCCs and RyRs. Stern [85] showed that these *local control models* are consistent with the experimental data. In a local control model, the choice of LCC and RyR openings is made essentially independently in each dyad, and the dyads couple only weakly via myoplasmic Ca^{2+} concentration. When an LCC opens, its opening determines local dyadic Ca^{2+} concentration, and thereby state of the LCC influences states of all RyRs close-by. Hence, the state of a RyR is statistically correlated with that of LCCs located in the same dyad. Because of this, bulk SR Ca^{2+} release is not a unique function of macroscopic $I_{Ca,L}$, even when microscopic $I_{Ca,L}$ is the sole mediator of SR Ca^{2+} release [85], but it depends on both open probability of LCCs as well as on unitary LCC current (not only on their product, that is, on macroscopic $I_{Ca,L}$).

This interplay between the LCC and RyR states together with driving force at different membrane potentials results a shift between peak fluxes through RyRs and LCCs [85, 34]. The shift between peak fluxes through RyRs and LCCs has also been observed experimentally [103], and it emerges naturally in a local control model, but not in a common pool model.

Given the issues with common pool models, it is of importance that an

[1]The guinea pig ventricular myocyte model of Luo and Rudy [57] assumed that the whole-cell SR Ca^{2+} release depends directly on the whole-cell L-type calcium current. The cardiac dyad was not included as a compartment in the Luo-Rudy model [57], and their approach is best described as the *hybrid approach*.

integrative myocyte model describes EC coupling based on a local control model of CICR. To improve on the common pool model of Winslow et al. [106], Greenstein and Winslow [34] formulated a stochastic, integrative model of a cardiac myocyte based on the local control hypothesis [85] (and on Rice et al. [75]). In the Greenstein and Winslow model [34], a subset of 12,500 dyads of 20 RyRs and 4 LCCs each were simulated and the resulting Ca^{2+} fluxes were scaled to correspond to the physiological 12,500 dyad case. In the local control model of Greenstein and Winslow [34], gating of RyRs depended on local Ca^{2+} concentration in the dyadic cleft (each cardiac dyad in this model was divided into four interconnected dyadic clefts) in which the RyR was located. The model reproduced the graded release of Ca^{2+} from the SR, the experimentally observed shape of the EC coupling gain [103], and the shift between peak Ca^{2+} fluxes through LCCs and RyRs. Thus, Greenstein and Winslow [34] showed that an integrative model based on the local control hypothesis of Stern [85] provides a more detailed picture of EC coupling than a common pool model.

The rapid equilibrium approximation [39, 32] provides a computationally efficient simplification of the computationally heavy approach of Greenstein and Winslow [34]. The main innovation of Hinch et al. [39] was the use of the rapid equilibrium approximation of Ca^{2+} concentration in the dyad separately for each state of the compound Markov model of RyR and LCC kinetics. In their model, Ca^{2+} concentration was a function of Ca^{2+} fluxes but not time (unlike in Greenstein and Winslow [34]). This removed the dependence of transition rates of the Markov models describing RyR and LCC gating on dynamical dyadic Ca^{2+} concentration and thereby enabled the calculation of Ca^{2+} dependent transition rates without explicit simulation of Ca^{2+} concentrations. This enabled a significant improvement in simulation speed. A slight discrepancy in membrane potential is induced by this approximation, however, the difference is negligible [90]. Greenstein et al. [32] demonstrated that a model of CICR based on the rapid equilibrium approximation can be integrated into an integrative model of AP in canine cardiac myocytes.

4.2 Spatial models of the cardiac dyad

CICR depends on free Ca^{2+} concentration in a strictly constrained space, the cardiac dyad. Since Ca^{2+} diffusion depends on geometry of the cardiac dyad, the geometry of the dyad may have a significant influence on CICR. None of the integrative models described so far has investigated spatial Ca^{2+} concentration differences in the dyad, nor did they examine the impact of

the spatial extension of protein structures in the dyad on EC coupling gain.

Soeller and Cannell [82] investigated Ca^{2+} dynamics in an empty, cylindrical dyad by solving the electrodiffusion equation for the Ca^{2+} concentration profile. To partially account for molecular structures present in the cardiac dyad, Soeller and Cannell [82, 14] scaled the diffusion coefficient down. Their results showed that electrostatic potential due to phospholipid headgroups on the sarcolemma reduces concentration of free Ca^{2+} ions in the dyad by a factor of approximately 10. Their subsequent work extended the analysis to RyR opening [14], however, neither model is as such suitable for integrative studies.

Langer and Peskoff [52] examined Ca^{2+} diffusion in the cardiac dyad, essentially in a similar way as Soeller and Cannell [82]. In a following study [73], they embedded the model in a larger context of sarcomere. Langer and Peskoff [52, 73] investigated the cardiac dyad, in which box-shaped RyR structures were placed, using numerical methods to solve the diffusion equation in the dyad. Like the model of Soeller and Cannell [82], models of Langer and Peskoff [52, 73] are not suitable for integrative studies.

The general predictions of Langer and Peskoff [52, 73] and of Soeller and Cannell [82, 14] are that Ca^{2+} influx via an LCC increases dyadic Ca^{2+} to tens μmol/L concentration very rapidly following opening of the LCC; and that Ca^{2+} release from RyRs is a very sensitive function of the spatial clustering of RyRs, and position of RyRs relative to the LCC.

Hinch et al. [40] solved analytically the equilibrium Ca^{2+} concentration profile in an empty cylindrical dyad in the presence of electrostatic potential. They essentially rederived the steady state results of Soeller and Cannell [82] analytically instead of numerical simulations used in [82]. While Hinch et al. [40] showed that analytical methods can be used to investigate Ca^{2+} concentration profile in the dyad, they did not proceed to include protein structures in the dyad or examine macroscopic properties of a cardiac myocyte.

Stern et al. [87] examined the mechanisms of CICR in detail in a model of Ca^{2+} dynamics in the dyad without protein structures, employing both the rapid equilibrium approximation and numerical simulations. Stern et al. [87] found that one activating Ca^{2+} binding site per RyR is not sufficient for stable CICR, and that either strong Ca^{2+} inactivation of RyRs or allosteric interaction of neighboring RyRs is required for a stable CICR.

Contrary to the typical assumption of modeling that the dyad is an empty space, a large portion of the dyadic volume is occupied by large proteins, mostly by RyRs [10]. All above articles examined an empty dyad or described the protein structures as simplistic structures. Since electrostatic potential due to lipid head-groups on the sarcolemma reduces the already low number of free Ca^{2+} ions in the dyad, noise in the Ca^{2+} signal in CICR may be

significant. How these issues influence each other, and what is their combined influence on CICR has only recently been probed in the literature.

4.3 The small number of Ca^{2+} ions in the dyad

Recently, it has been recognized that models tracking individual ions and molecules in biochemical networks are necessary due to the small number of signaling molecules [4, 88, 11]. Results of Bhalla [11] suggested that the traditional mass-action law ceases to be computationally reliable for volumes below 10^{-15} liter (that is, a femtoliter). Bers [10] estimated that in CICR only relatively few free Ca^{2+} ions (that act as second messengers in EC coupling) are present in the cardiac dyad at any time, even at peak density. This suggests that a high noise level may be associated with CICR. None of the models briefly described in Sections 4.1 and 4.2 took into account the small number of free Ca^{2+} ions mediating CICR in the dyad.

Koh et al. [49] formulated an MCell [88] based model of Ca^{2+} dynamics in an empty cardiac dyad. In their model, each Ca^{2+} ion was simulated individually. Koh et al. [49] found that peak Ca^{2+} concentration is almost independent of the dyad radius, however, height of the dyad had a major impact on the peak Ca^{2+} concentration. The results of Koh et al. [49] suggested that free Ca^{2+} ion concentration in the dyad is significantly higher than assumed in the previous studies. This is partly due to the fact that a single Ca^{2+} ion corresponds to concentration of 13 μmol/L in the dyad with radius 100 nm, and partly due to the fact that Koh et al. [49] did not consider electrostatic potential due to phospholipid head groups that reduces the number of free Ca^{2+} ions in the cardiac dyad.

In the MCell-based model of Koh et al. [49], Ca^{2+} ions move according to Brownian motion (random walk) in the dyad in the absence of molecular structures and electrostatic potentials. As shown by Soeller and Cannell[82], electrostatic potential significantly affects free Ca^{2+} concentration in the cardiac dyad. Hence, the method of Koh et al.[49] does not describe Ca^{2+} dynamics in the dyad sufficiently accurately to enable understanding of the impact of noise in Ca^{2+} signaling on EC coupling.

4.4 Spatially- and molecularly-realistic models of the dyad

To fully address the impact of the small number of Ca^{2+} ions responsible for triggering CICR, a model must incorporate geometry of proteins in the

cardiac dyad, electrostatic potential due to headgroups on the sarcolemma, and individually tracked Ca^{2+} ions. Article III investigated CICR and EC coupling gain by formulating a spatially realistic model of the dyadic Ca^{2+} dynamics in which individually simulated Ca^{2+} ions move under the influence of electrostatic potential. Despite the fact that recent advances in cryoelectromicroscopy have brought ever more detailed picture of RyR (e.g., Sharma et al. [80]), no previous computational model has examined the impact of realistic RyR protein structures on CICR. The model of article III is briefly reviewed in the following.

In article III, the cardiac dyad was approximated as a box of dimensions $200 \times 200 \times 15$ nm. Boundaries representing sarcolemma and the SR membrane were assumed to be reflecting in the sense that Ca^{2+} ions cannot cross these membranes. The dyad-myoplasm interface (Figures 2.1 and 2.3) was approximated as an absorbing membrane, that is, any Ca^{2+} ion hitting this boundary was removed from the simulation. To incorporate realistic molecular structures, RyR structures were modeled based on cryoelectromicroscopy data [81], while both LCC structures [100] and CaM structures [50] were modeled based on crystal structure data. These protein structures were discretized and incorporated in the model as lattice points not admissible for Ca^{2+} ions to diffuse in. LCC-structures were placed on the sarcolemma, CaMs tethered to LCCs, and RyRs resided as quasicrystal arrays (Fig. 1 in article III) apposed to LCCs.

To investigate the movement of discrete Ca^{2+} ions, the local equilibrium approximation of Wang et al. [99] (reviewed in Appendix A) was used in article III. In this approach, continuous movement of a Ca^{2+} ion in the presence of realistic molecular structures and a potential due to phospholipid headgroups was discretized to a movement on a lattice (with 1 nm lattice spacing), which can be approximated as a continuous-time discrete-state Markov process. Kinetic models describing LCC and RyR gating were based on previous, experimentally-verified models in the literature: the four-state kinetic model of RyR gating was based on Stern et al. [87], and the 11-state kinetic model of LCC gating was based on Winslow et al. [106]. To account for ion channel activation (RyRs) and inactivation (RyRs and LCCs) due to binding of Ca^{2+} ions, transition rates of kinetic models describing the ion channels were modified to depend on binding status of the corresponding Ca^{2+} binding sites. When a suitable number of Ca^{2+} binding sites of an LCC or RyR were occupied, Ca^{2+}-dependent state transitions of the corresponding ion channel were enabled. Finally, movement of Ca^{2+} ions in the dyad and gating of ion channels were in this model combined into a single high-dimensional continuous-time discrete-state Markov process, which was in article III simulated stochastically.

Novel features of the model described in article III included simulation of the dynamics of individual Ca^{2+} ions and ion channels in a realistic spatial setting in the presence of realistic noise sources: gating noise, and signaling noise due to Ca^{2+} ion movement and binding reactions. The model also enabled investigation of macroscopic properties of a myocyte depending on CICR, such as EC coupling gain, starting from microscopic variables.

The results of article III suggest that RyR structures "funnel" Ca^{2+} ions toward binding sites on RyRs. Funneling occurs because the presence of large RyR structures increases the probability that a Ca^{2+} ion binds to an activating binding site, which increases the probability that the RyR opens. As shown in article III, the shape of RyR protein structures increases EC coupling gain significantly. Another finding of article III was that the presence of electric potential due to lipid head-groups reduces EC coupling gain, partially due to associated increased noise level in Ca^{2+} signaling (see Sec. 5.2 for further discussion). It was also found that the relative placement of protein structures in the dyad is functionally very important: the exact placement of LCCs apposed to RyRs influences CICR in the dyad. In particular, the position of binding sites on the RyR protein structures relative to the source of Ca^{2+} influx significantly modulates EC coupling gain (Fig. 7 in article III).

4.5 Integrative, spatially-realistic models of the dyad

Spatially-detailed models of the cardiac dyad are rarely suitable for inclusion in an integrative model of a cardiac myocyte. This, however, is of crucial importance to the development of spatially-realistic, integrative models of the heart [107]. To develop a spatially-detailed integrative model of CICR in the cardiac dyad, a model was formulated in article IV based on the rapid equilibrium approximation of Ca^{2+} concentration profiles in the cardiac dyad and on biophysically detailed Markov models of ion channel kinetics.

A characteristic time a Ca^{2+} ion spends in the dyad is a few microseconds, while each state of an ion channel typically lasts for hundreds or thousands of microseconds. Hence, Ca^{2+} diffusion is several orders of magnitude faster than ion channel gating in the dyad. This suggests that the rapid equilibrium approximation of Ca^{2+} probability density provides a good approximation to a more detailed model simulating individual Ca^{2+} ions, when a large number of Ca^{2+} ions are present in the dyad. While this is not necessarily the case in Ca^{2+} trigger, rapid equilibrium approximation may nevertheless work

sufficiently well in the dyad.

In article IV, a starting point for modeling Ca^{2+} concentration profile was the rapid equilibrium approximation of a Fokker-Planck equation

$$\frac{\partial P(t,x)}{\partial t} = D\Delta P(t,x) + \sum_{k=1}^{3n} \frac{\partial}{\partial x_k}\left[P(t,x)\frac{\partial U(x)}{\partial x_k}\right], \quad P(t_0,x) = F(x), \quad (4.1)$$

describing the probability $P : \mathbb{R}^{3n+1} \to \mathbb{R}$ of finding n Ca^{2+} ions at positions $x \in \mathbb{R}^{3n}$ at time $t \in \mathbb{R}$. In equation (4.1), $\Delta = \sum_{k=1}^{3n} \partial^2/\partial x_k^2$ is the Laplacian defined on twice diffentiable functions, and $D \in \mathbb{R}^+$ is the Ca^{2+} diffusion coefficient. Function $U : \mathbb{R}^{3n} \to \mathbb{R}$ describes both the potential inside the dyad due to negatively-charged phospholipid headgroups on the sarcolemma [82, 52] and interactions of Ca^{2+} ions. Distribution $F : \mathbb{R}^{3n} \to \mathbb{R}$ describes the initial positions of Ca^{2+} ions.

Assuming potential U does not include $Ca^{2+} - Ca^{2+}$ interactions, equation (4.1) reduces in equilibrium to a linear second-order partial differential equation

$$(L\rho)(y) = 0, \quad (4.2)$$

where L is an operator defined by $(Lu)(y) = D\Delta u(y) + \sum_{k=1}^{3} \frac{\partial}{\partial y_k}\left[u(y)\frac{\partial U(y)}{\partial y_k}\right]$ on $C^2(\mathbb{R}^3, \mathbb{R})$. Probability P of all Ca^{2+} ions is in this formulation replaced with probability density ρ of a single Ca^{2+} ion. Probability density ρ can be interpreted as a "concentration", however, it describes the expected density of Ca^{2+} ions rather than the actual number of Ca^{2+} ions present in a volume.

A model of CICR must describe the entry of Ca^{2+} ions into the dyad. Since equation (4.2) does not account for the entry of Ca^{2+} ions, a source term must be included. Assuming that probability mass enters the dyad continuously, a source term is given by, e.g., $J\delta(y - z_k)$, where $J \in \mathbb{R}$ is magnitude of the influx, z_k is the position of Ca^{2+} source k, and δ is the Dirac δ-distribution. Under these assumptions, Ca^{2+} concentration profile is obtained by solving equation

$$(L\rho)(y) = \sum_k J_k \delta(y - z_k), \quad (4.3)$$

where $y \in \mathbb{R}^3$, and J_k is the magnitude of Ca^{2+} flux through source or sink k. In the absence of potential U, equation (4.3) reduces to a Poisson equation. To investigate Ca^{2+} concentration in the cardiac dyad, equation (4.3) is solved in a cylindrical space (with appropriate boundary conditions) representing the dyad. In article IV, it was assumed that the boundaries representing sarcolemma and the SR membrane were reflecting, while boundary on the dyad-myoplasm interface was absorbing. Realistic shapes of the boundaries

are rather complex due to the shape of the proteins, mainly RyRs, which requires that equation (4.3) must in practice be solved numerically.

In the CICR models of article IV, an ion channel consisted of two parts: a kinetic model describing kinetics of ion channel states; and a model of activating and inactivating Ca^{2+} binding sites. The kinetic model was described as a compound RyR-LCC Markov model, state of which determined Ca^{2+} fluxes through the ion channels. Transition rates of the kinetic model were determined by the states of the associated binding sites, which depended on Ca^{2+} concentration ρ near each Ca^{2+} binding site. Hence, if equilibrium Ca^{2+} concentrations at the binding sites are known, all transition rates in a compound RyR-LCC Markov model can be calculated independently of time, which enables a computationally-efficient, integrative description of CICR. To make the model computationally efficient, Ca^{2+} concentration profiles must be calculated efficiently. Since equation (4.3) is linear, steady state Ca^{2+} concentration profile for any flux configuration can be computed based on a few elementary concentration profiles, which can be precomputed before the actual simulation.

The above considerations provide a method to develop a spatially-realistic, computationally-efficient model of CICR in the cardiac dyad based on the local control hypothesis. In article IV, a model suitable for inclusion in an integrative model of a cardiac myocytes was developed. It was based on the above method in the case $U = 0$. Article IV showed that such a model reproduces the physiologically important properties of EC coupling, in particular the graded release of Ca^{2+} from the SR and the decreasing shape of EC coupling gain. The main physiological findings of article IV were that the geometry of RyR protein structures have a major impact on CICR by increasing EC coupling gain, and that the shape of the RyR protein enables binding sites to more robustly detect Ca^{2+} ions entering from the apposing LCC. These findings agree with the results of article III.

The method described above is general in the sense that it enables the use of equilibrium Ca^{2+} concentration profiles from any model of the dyadic Ca^{2+} dynamics, e.g. Soeller and Cannell [82], in an integrative model of CICR. The CICR models derived in article IV show that it is feasible to incorporate realistic protein structures, binding of Ca^{2+} ions to activating and inactivating binding sites, electrostatic potentials, and concentration profiles into a computationally efficient integrative model of a cardiac myocyte. In this sense, the method enables the completion of the development program of myocyte models outlined in Winslow et al. [107] stating that a model of CICR with the above properties should be developed. In addition to modeling CICR, the method is suitable for other situations, such as describing potassium and calcium dynamics in BK_{Ca}-CaV nanodomains in neural cells[9].

Chapter 5

Noise and the macroscopic properties of a cardiac myocyte

Noise can be defined as random variations of one or more measurable characteristics of any entity, such as voltage, or current. In cellular processes, noise is present due to many reasons, e.g., thermal noise is a manifestation of random movement of molecules, and shot noise (e.g., gating noise) is a result of stochastically occurring discrete events.

Noise is often thought to only "blur" the evolution of a dynamical system, but not influence average properties of the system. This indeed is the case in a linear system [3, 55], however, this may not be true in a *non*-linear system: the presence of noise in a dynamical non-linear system may influence average properties and induce transitions absent in a deterministic model [55, 78]. For example, Samoilov et al. [78] show that in a futile enzymatic cycle (a biochemical reaction in which a substrate is converted to product by a forward enzyme and then can be converted back to substrate by a reverse enzyme), noise may induce bistability which is absent in a corresponding deterministic model. In some cases, evolution has even enabled certain cellular processes to take advantage of noise by utilizing stochastic resonance [76].

Small number of signaling molecules may induce a significant noise level to a cellular process dependent on this signaling [11]. Effects of this signaling noise are particularly likely to be found in subcellular signaling pathways, in which a relatively small number of constituent molecules interact non-linearly. This is the case in many second messenger systems, such as CICR. Since this kind of signaling pathways often play a crucial role in cellular processes, it is of significant interest to investigate how signaling noise influences the cellular processes, in particular, the physiology at the macroscopic level.

The impact of noise on a non-linear dynamical system is an important area of research, since many physiological systems evolve in the presence of

noisy drivers. The following sections investigate the impacts that noise may have on a cardiac myocyte.

5.1 Distribution of APDs

APD measuring the duration of an AP is an important determinant of the presence of life-threatening EADs. In any recording of membrane potential of a cardiac myocyte, noise is present in the measured voltage [38]. This noise is known as voltage noise and it is mainly due to gating noise of ion channels [112]. Beat-to-beat variation of APD is likely noise-induced [112]. There are two main approaches to explore the impact of noise on APD: (1) use of a stochastic ionic model (e.g., Wilders and Jongsma [104]); and (2) application of stochastic differential equations (e.g., Clay and DeHaan [18]).

Wilders and Jongsma [104] examined the impact of stochasticity on a sinoatrial node cell. Their main result was that variation in interbeat-interval in the sinoatrial node cells is consistent with the stochastic open-close kinetics of membrane ion channels.

Clay and DeHaan [18] applied stochastic differential equations to describe the distribution of interbeat-intervals in embryonic chick ventricular myocytes, and showed that the distribution of interbeat-intervals in chick heart-cell clusters is well described by a diffusion process with a constant drift and a constant diffusion coefficient representing the noise level.

Of these two approaches, an ionic model is preferable, because it enables a more biophysically detailed description of gating noise. However, stochastic differential equations enable analytical characterization of the response of APD to varying noise levels, which is not possible using an ionic model.

The typical influence of voltage noise on APD was investigated in article II, where it was shown that a higher noise level increases average APD in two different models of the AP in cardiac myocyte. Similar increases were observed both in the ionic model of Greenstein and Winslow [34], and in a model based on a diffusion process (article II). This is explained in more detail in the following sections.

5.1.1 The deterministic case

First, let us analyze the impact of a single fluctuation on average APD. Assuming a myocyte is initially at voltage x at the start of the plateau phase of an AP, and that the current-voltage relationship is described by function

$I : \mathbb{R} \to \mathbb{R}$ mapping voltage to membrane current, APD is given by

$$T_x = \int_a^x \frac{C_m\, dz}{I(z)}, \tag{5.1}$$

where a is the target voltage corresponding to a voltage where APD is calculated, and C_m is specific membrane capacitance. Then, the average response of APD, denoted here by ΔT_x, to a symmetric voltage fluctuation $x \pm \varepsilon$ in the initial voltage is given by

$$\Delta T_x = \frac{1}{2}(T_{x+\varepsilon} + T_{x-\varepsilon}) - T_x = -\frac{1}{2}\left(\int_{x-\varepsilon}^{x} \frac{C_m\, dz}{I(z)} + \int_x^{x+\varepsilon} \frac{C_m\, dz}{I(z)}\right). \tag{5.2}$$

If the $I(V)$ function is positive and increasing (which corresponds to repolarization of voltage at a rate that is decreasing with time, since voltage decreases with time), the second integral in equation (5.2) dominates over the first one, that is, $\Delta T_x < 0$. Under these conditions, APD is on average reduced in response to the symmetric fluctuation in the initial voltage. Similarly, if the $I(V)$ function is positive and decreasing (which corresponds to repolarization of voltage at a rate that is increasing with time), the first integral dominates over the second one, that is, $\Delta T_x > 0$, and on average APD is increased in response to the symmetric fluctuation $x \pm \varepsilon$ in the initial voltage. Hence, the sign of I' influences the noise response of APD asymmetrically, even when the fluctuation in the initial voltage is symmetric. This suggests that noise may have a non-trivial impact on APD in the presence of a non-linear current-voltage relationship.

5.1.2 The general case

Stochastic differential equations enable investigation of noise response of APD in a more general setting than the method described above. In particular, the impact of noise on APD can be approximated by representing membrane potential V_t as a stochastic process

$$dV_t = -I(V_t)dt/C_m + \sigma(V_t, t)dB_t, \qquad V_0 = v_0, \tag{5.3}$$

defined in complete filtered probability space $(\Omega, \mathcal{P}, \{F_t\}, \mathcal{F})$ [69], and considering the stopping time $\tau = \min\{t : V_t \leq a\}$. Above $\sigma : \mathbb{R}^2 \to \mathbb{R}$ is the diffusion coefficient, and B_t is the standard Brownian motion [69]. When voltage a is chosen appropriately, stopping time τ represents APD. Functions I and σ can then be estimated from experimental measurements or, in their absence, from simulations in a biophysically detailed model.

The method of Alvarez [3] can be employed to investigate the properties of the Laplace transformation of stopping time τ and thereby the general properties of APD. It can be shown that the Laplace transform $E_x[e^{-r\tau}]$ of stopping time τ (that is, APD) can be represented as $\varphi(y)/\varphi(x)$ (see Borodin and Salminen [12]; Ito and McKean [46]), where φ is the fundamental decreasing solution of equation

$$\frac{1}{2}\sigma^2(z)\varphi''(z) - I(z)\varphi'(z)/C_m - r\varphi(z) = 0. \tag{5.4}$$

Hence, to investigate the Laplace transform of APD, it suffices to examine φ. A change in noise level (that is, σ) influences φ in a specific way determined mainly by the sign of I' (article II). Since the Laplace transform of τ determines all moments of APD, the fundamental decreasing solution φ can be used to investigate the response of APD to a change in noise level.

The results of article II suggest that an increased level of voltage noise will on average increase APD and skew the distribution of APDs toward long intervals in ventricular myocytes, since the $I(V)$ function is typically decreasing as a function of voltage during the plateau phase of an AP. This result is general in the sense that it holds for almost any decreasing $I(V)$ function. In addition, it is likely that the result can be generalized to any noise process with a symmetric distribution.

In article II, it was shown that APD distribution of the model of Greenstein and Winslow [34] can to a high degree be reproduced by a diffusion process. In both models, an increase in noise level led to increases in both average and skewness of APD distribution, but to a decrease in mode of APD distribution (Fig. 3 in article II). The increase in skewness due to an increase in voltage noise level is consistent with the observation of EADs in response to a higher gating noise level in article I.

5.2 Noise due to the small number of Ca^{2+} ions in the cardiac dyad

During CICR, only 1-100 free Ca^{2+} ions are present in the dyad at any given time, even at the peak density when RyRs are open (see Bers[10], and Fig. 8 in article III). A significantly smaller number of Ca^{2+} ions are present during the initial phase of CICR, when Ca^{2+} ions entering through LCCs induce opening of RyRs. Nevertheless, CICR and EC coupling are robust processes, as is manifested in the fact that the heart operates continuously for 80 years or more pumping 5-25 liters of blood each minute. Detailed investigation of

these issues was the topic of article III, where the impact of realistic protein structures on EC coupling gain was also examined.

At 0 mV, approximately 300 Ca^{2+} ions enter the dyad through an open LCC each millisecond. The typical open time of an LCC is 0.5 ms, and hence the typical number of Ca^{2+} ions entering the dyad is 150 per LCC opening at 0 mV. The number of free Ca^{2+} ions is significantly reduced by electrostatic potential due to phospholipid headgroups on sarcolemma, which may leave only a few free Ca^{2+} ions to trigger RyR opening. These Ca^{2+} ions leave the dyad so rapidly that on average less than one free Ca^{2+} ion is assumed to be present in the dyad [10]. Since an opening of a RyR requires simultaneous binding of 2-4 Ca^{2+} ions, it seems that CICR cannot be a robust process.

Unlike the above simplistic computation suggests, CICR is a robust process, as shown by the results of article III suggesting that 20-50 free Ca^{2+} ions suffice to mediate CICR. An important factors in this are the large number of dyads in a cardiac myocyte, relative locations of the small height of the dyad, and the RyR protein structures that "funnel" Ca^{2+} ions to binding sites and thereby suppress the noise inherent in Ca^{2+} signaling. The presence of electrostatic potential due to phospholipid headgroups on sarcolemma reduces EC coupling gain and increases noise level in Ca^{2+} signals associated with the CICR.

During an LCC opening the number of free Ca^{2+} ions in the dyad fluctuates wildly (Fig. 8 in article III). Due to these fluctuations and the fact that a single Ca^{2+} ion represents Ca^{2+} concentration of 13 μmol/L (in a cylindrical dyad with radius 100 nm), models employing mass action law significantly underestimate the peak Ca^{2+} concentration during an LCC opening.

Since Ca^{2+} ions induce RyR opening, a strong positive feedback is present in CICR (essentially by definition). Positive feedback will amplify any fluctuation in Ca^{2+} signal, unless kept in check somehow. Mechanisms that keep CICR stable[1] are known to operate during CICR: (1) Ca^{2+}-inactivation of RyRs; (2) Ca^{2+}-inactivation of LCCs; (3) requirement that multiple Ca^{2+} ions bind to a RyR before it opens [111]. However, it has not been previously shown in a mathematical model that these mechanisms are sufficient for a stable and reliable CICR in the presence of noise in the Ca^{2+} signal due to discreteness of Ca^{2+} ions. The article III shows that mechanisms (1)-(3) are sufficient to ensure stable CICR when only 20-50 free Ca^{2+} ions mediate CICR.

Entry of Ca^{2+} ions through an open LCC triggers opening of RyRs located on the SR membrane apposed to LCCs. Through a single open RyR,

[1] In addition, allosteric interactions between RyRs are known to be present, however, these interactions are not considered in this thesis.

approximately 4,000 Ca^{2+} ions enter the dyad each millisecond [101]. Hence, signal-to-noise ratio of Ca^{2+} signal is significantly higher after one or more RyRs open, and signaling noise influences mainly the initial phase of CICR.

In continuum approximation, a Ca^{2+} ion (more precisely, a non-zero Ca^{2+} concentration) is always present near a binding site if average dyadic Ca^{2+} concentration is non-zero, which is not the case when Ca^{2+} ions are discrete. Hence, signaling noise in Ca^{2+} trigger likely influences EC coupling gain. One way to investigate the impact of signaling noise is to scale both Ca^{2+} influx via LCCs and RyRs, and the diffusion coefficient by the same factor. Since a higher (respectively, lower) Ca^{2+} influx compensates for the reduction (increase) in dyadic Ca^{2+} concentration due to a higher (lower) diffusion coefficient, this method enables investigation of the noise level in Ca^{2+} signaling on CICR. In article III, it was shown (Fig. 12 in article III) that more noisy Ca^{2+} signaling (a lower Ca^{2+} diffusion coefficient coupled together with a lower Ca^{2+} influx) in CICR reduced EC coupling gain. Similarly, less noisy Ca^{2+} signaling increased EC coupling gain.

The results of article III support the view that gating noise is the main source of noise in CICR, however, Ca^{2+} signaling noise due to the small number of Ca^{2+} ions does contribute by reducing EC coupling gain. In summary, article III showed that CICR is robust at the whole-cell level even though only a few free Ca^{2+} ions are responsible for triggering further Ca^{2+} release from RyRs in each dyad.

5.3 Gating noise and EADs

Repolarization of a cardiac myocyte is a precarious process. While many different currents orchestrate repolarization, only a few channels of each type are open at any given time [59]. Hence, small changes due to opening/closing of a handful of individual channels may pervert repolarization.

A rather common type of repolarization abnormality is a spurious secondary depolarization of an AP known as an early after-depolarization (EAD). EADs occur during phase 2 or phase 3 of an AP, however, these two occurrences may be due to different mechanisms [10]. Medical importance of EADs stems from their association with polymorphic tachycardia [10], which is a frequent precursor to sudden cardiac death in heart failure patients [72].

Experimental data suggest that signaling events such as CaMKII phosphorylation and β-AR stimulation induce EADs [23, 98]. Mazur et al. [60] showed that blockers of CaMKII and PKA eliminate EADs as well as torsades de points. Since repolarization of the AP depends on only a few open ion channels, it is likely that gating noise influences repolarization [112, 104].

During the plateau phase of the AP, membrane current is dominated by inward Ca^{2+} current and outward potassium currents in a delicate balance. Cardiac LCCs have four distinct gating modes [37, 110] known as 0, 0a, 1 and 2. The typical open state in mode 1 has 0.5 ms duration, while the high-activity gating mode 2 has a relatively long open time of 5 ms [110]. Silent gating mode 0 and and low activity mode 0a do not contribute significantly to Ca^{2+} current. Physiological role of mode 2 gating is likely to enhance heart contraction under β-AR stimulation, that is, under "fight-or-flight" conditions. Certain signaling events that promote LCC phosphohorylation also promote mode 2 gating of LCCs. In particular, PKA-mediated phosphorylation of LCC increases both the fraction of LCCs available for gating as well as the ratio of LCCs gating in mode 2. Similarly, CaMKII phosphorylation increases the ratio of LCCs gating in mode 2. Motivated by this, article I examined how gating noise due to LCCs influences action potential duration and shape using a stochastic model of β-AR stimulation in a cardiac myocyte.

The basis for the model in article I was formulated by Greenstein et al. [33], who extended the Greenstein-Winslow model [34] of the canine ventricular myocyte to include the effects of β-AR stimulation by 1 μmol/L isoproterenol. β-AR stimulation increases the availability of LCCs and thereby the availability of the cardiac dyads from 12,500 in the baseline to 30,000 available dyads (out of the total 50,000 dyads present in a myocyte) [33]. In the model, β-AR stimulation induced PKA-mediated phosphorylation of LCCs, which shifts LCCs to high-activity gating mode 2. Finally, β-AR stimulation enhanced SERCA rate by factor 3.3, increased I_{Ks}, and reduced inactivation of I_{Kr}. Incorporation of these phosphorylation-dependent effects in the model [34] yielded changes of action potential and Ca^{2+} transients in agreement with those measured experimentally [33].

The presence of LCCs gating in mode 2 increased the heterogenity of ion channels responsible for L-type calcium current, which increased gating noise level associated with this current. A higher gating noise level may influence AP morphology, which was explored by an ionic model of the cardiac AP in article I. Article I showed that an increased noise level in L-type calcium current due to the presence of an increased ratio of LCCs gating in mode 2 may induce EADs. EADs occurred when an increased ratio of LCCs gated in mode 2 due to two factors: (1) deterministic prolongation of APD due to an increased Ca^{2+} influx; and (2) increased gating noise level which generated noise-induced formation of EADs. In simulations, frequency of EADs depended on the ratio of LCCs gating in mode 2, with a higher ratio of LCCs gating in mode 2 inducing a higher frequency of EADs. The occurrence of EADs was random, which was shown by the finding that changing random

number seed in simulation during a late phase of the plateau before an EAD formed was sufficient to remove the EAD or induce a second EAD.

The observation of stochastic formation of EADs is supported by the fact that APD distribution in the model of Greenstein and Winslow [34] (on which the β-AR model [33] is based) becomes skewed toward long intervals at high gating noise levels (article II), which predisposed a myocyte to EADs. In addition, it is a well documented fact that noise in bistable systems induces transitions absent in a corresponding deterministic system [55]. Since a myocyte is known to be a bistable system in the sense that rather small modifications of membrane currents may lead to secondary depolarizations [113], the finding of EADs as a results of gating noise is consistent with previous studies of noise in bistable systems (e.g., Lindner et al. [55]).

The finding of stochastic induction of EADs due to mode 2 gating of LCCs may also be relevant for heart failure. It is known that AP shapes in failing myocytes are more variable than in normal myocytes [71]. In a failing myocyte, fewer LCCs are available to gate but the total current density through LCCs is unchanged [16]. This suggests that a higher ratio of LCCs gate in mode 2 in heart failure than under normal conditions. If this indeed is the case, increased gating noise level due to mode 2 gating of LCCs may contribute to increased frequency of EADs in failing myocytes.

Chapter 6

Discussion

In articles I-IV included in this thesis, mathematical models were constructed to investigate cardiac myocytes, Ca^{2+} dynamics in the cardiac dyad, and how noise due to various sources modulate properties of a myocyte. The main results of the thesis are discussed in the following sections.

6.1 The impact of noise on a cardiac myocyte

Suppression of noise in cellular processes is energetically expensive. Hence, it is likely that each organism operates at a maximal noise level consistent with its survival [1]. This suggests that under normal conditions, operation of an organism is robust against noise. Under abnormal conditions this may not be the case: for example, it is known that under heart failure conditions, variability of AP shape increases significantly [71], which suggests that random signals (e.g., gating noise) influence functioning of a myocyte more than under normal conditions. While this AP variability is not only due to noise sources examined in this thesis, it is consistent with the results of this thesis suggesting that noise may have a significant impact on the function of the heart, in particular under pathological or exceptional conditions.

Article I showed that noise due to mode 2 gating of LCCs may under β-AR stimulation induce EADs. Article II proved that a higher noise level in a diffusion process model induces prolongation of average APD as well as a higher probability of hitting a higher voltage, that is, of inducing an EAD. These results are consistent with the general observation that excitable bistable systems exhibit noise-induced transitions [55].

Gating noise due to ion channels induces beat-to-beat variability to APD. In Zaniboni et al. [112], it was found that APD is approximately normally distributed. However, even a rather simple model based on stopping time of

a diffusion process (article II) suggests that the distribution of APDs should be skewed toward long durations. Similarly, in the biophysically detailed model of cardiac AP of Greenstein and Winslow [34], the APD distribution is skewed toward long durations (article II). These results suggest that APDs in cardiac myocytes are not necessarily normally distributed, and that the distribution of APDs is likely skewed to some degree. If this is not the case, a mechanism reducing the skewness of the APD distribution must be present in a myocyte.

6.2 Impact of noise in CICR on EC coupling gain

A significant signaling noise is present in CICR due to the small number of Ca^{2+} ions and gating noise. How does robust EC coupling arise from noisy CICR, as was observed in article III? Firstly, approximately 12,500 cardiac dyads are present in a single myocyte, and the global Ca^{2+} release at the myocyte level is an integrated function of all dyadic Ca^{2+} release events. Secondly, as was shown in article III, the shape of RyR protein structures enables RyRs to robustly detect Ca^{2+} trigger, which increases EC coupling gain and attenuates the impact of noise on CICR. Thirdly, CICR couples negative feedback via Ca^{2+} inactivation attenuating noise together with positive feedback in CICR amplifying noise [55]. While additional mechanisms are likely present in a cardiac myocyte, these three mechanisms are sufficient for stable CICR at the cell level. The presence of a significant noise level sets constraints on possible mechanisms of CICR, e.g., the absence of negative feedback would disable CICR and break EC coupling since any fluctuation would result in an unstoppable Ca^{2+} release.

Bhalla [11] argued that at volumes below 1 femtoliter (10^{-15} l), the commonly used mass action law becomes unreliable for modeling signaling networks. Volume of the cardiac dyad is 10^{-3} femtoliters, which suggests that at a single dyad level, mass action law and the traditional concentration approach do not work. Even the compound volume of all available cardiac dyads present in a myocyte is only approximately 10 femtoliters, which is close to the 1 femtoliter threshold of Bhalla [11]. Nevertheless, according to the results of article III, CICR has a significant noise component at the level of a single dyad, but whole-cell EC coupling is robust and EC coupling gain is less influenced by stochasticity at the whole-cell level.

CICR is not only observed in the cardiac muscle, but has been described in skeletal muscle [27], smooth muscle [36], parasympathetic neurons [7],

adrenocortical cells [109], and auditory and vestibular hair cells [53, 84]. Given the ubiquity of CICR, these results are of importance in many biologically important systems. EC coupling in skeletal and smooth muscle myocytes occurs in a different way from EC coupling in a cardiac muscle. In skeletal muscle LCCs couple mechanically to RyRs, while in cardiac myocytes no such mechanical coupling is known to occur. Hence, while CICR occurs in skeletal muscle it can be expected that Ca^{2+} signaling noise due to small number of second messenger Ca^{2+} ions is less important in skeletal muscle than in cardiac muscle. In smooth muscle cells, EC coupling occurs via RyR-driven CICR and IP_3-dependent receptors [10], which suggests that the results of this thesis also apply to smooth muscle cells.

6.3 Protein structures in the dyad

Biophysically detailed computational models of a ventricular myocyte should be based on experimental measurements and on anatomical data on real cellular geometry, whenever possible. Taking anatomical data into consideration is particularly important in modeling compartments in which significant protein structures compared to the volume are present, as is the case in the cardiac dyad. Computational models that take these issues into account are predictive and represent much more than just a summary of experimental data [45]. Computational models enable investigation of issues which are difficult to examine in experimental studies, e.g., the impact of the relative position of LCC to RyRs on EC coupling gain and how geometry of RyR protein structures influences CICR.

The results of articles III and IV suggest that protein structures may have a significant impact on CICR via two different mechanisms. Firstly, large RyR feet structures increase the probability that a Ca^{2+} ions binds to an activating binding site. Secondly, protein structures reduce the impact of Ca^{2+} signaling noise on CICR, which improves the reliability of CICR. These mechanisms enable a smaller Ca^{2+} signal to trigger CICR than is possible in the absence of RyR protein structures. The smallness of Ca^{2+} trigger reduces the energy consumption of a myocyte because any extra Ca^{2+} must be extruded from the myocyte, which is energetically more expensive than Ca^{2+} storage in the Sarcoplasmic Reticulum.

Another important aspect of protein structures is the exact placement of LCCs apposed to RyRs in the dyad. In article III, it was found that both the location of RyRs in the dyad and the location of Ca^{2+} binding sites on RyR surface influence EC coupling gain (Fig. 7 in article III). This suggests that the relative position of LCCs and RyRs may have a significant impact

on CICR. Interestingly, it has been argued that position of LCCs relative to RyRs is almost random [87]. Hence, noise due to the placement of LCCs relative to RyRs may influence EC coupling gain. It provides an attractive target for future investigations. In addition to noise sources analyzed in this thesis, local voltage noise due to, e.g., movement of gating charges is present in the dyad.

An issue related to protein structures in the cardiac dyad is the impact of mobile Ca^{2+} buffers facilitating Ca^{2+} diffusion out of the dyad. Immobile Ca^{2+} buffers do not influence steady-state Ca^{2+} concentration in the dyad, they only modulate the rate of approach to the steady-state Ca^{2+} concentration. In contrast, mobile Ca^{2+} buffers do influence the dyadic steady-state Ca^{2+} concentration, since mobile buffers are replenished from the myoplasm. The main mobile buffers found in the cardiac dyad are CaM and ATP [10]. In CICR, mobile Ca^{2+} buffers can facilitate Ca^{2+} diffusion from the dyad to myoplasm and thereby they reduce the already low number of free Ca^{2+} ions in the Ca^{2+} trigger. Given that the most likely concentration of mobile Ca^{2+} buffers is low, it is unlikely that mobile Ca^{2+} buffers would have a major impact on CICR. Mobile Ca^{2+} buffers were not investigated in article III, since it is not well known how many mobile buffers are present in the dyad and since the impact of mobile Ca^{2+} buffers is likely relatively small to Ca^{2+} buffering. Nevertheless, certain "mobile Ca^{2+}-buffers" (e.g., CaM and CaMKII) actually modulate function of LCCs and RyRs in the cardiac dyad, and they should be included in future models of Ca^{2+} dynamics in the dyad.

6.4 Multiscale approach

CICR is an important example of a general theme in biology - signaling within subcellular microdomains mediated by small numbers of molecules [10]. Signaling events associated with CICR have a profound influence on the cardiac electro-mechanical function at the level of cell and tissue, thus necessitating multiscale modeling approaches. In the multiscale approach, the aim is to link microscopic details (e.g., location of binding sites on a RyR molecule) to macroscopic details (e.g., properties of EC coupling gain). An integrative biophysically detailed cell model provides a prime example of the multiscale approach: each ion channel is a molecular machine operating in nanometer scale, while length of a mammalian cardiac myocyte is approximately 100 μm [57].

Human body consists of approximatively $1-10\times10^{13}$ cells [25]. The heart consists of $1-10\times10^{9}$ connective tissue cells and $2-8\times10^{9}$ heart muscle cells [2, 70]. Computational single-cell models can be coupled together to build a

tissue-level model, which can be used to provide quantitative understanding of whole-organ behavior in terms of sub-cellular function [107, 66, 45]. A model of an entire heart consisting of biophysically detailed models therefore spans length scales from the nm scale to the cm scale, that is, 8 magnitudes. A whole-heart model should represent a large subset of the approximatively 10^{10} individual cells present in the heart.

In integrative whole-heart modeling, there is always a trade-off between detail and computational tractability which necessitates constant development of cell models. An integrative whole-heart model cannot directly incorporate a model tracking individual Ca^{2+} ions in the dyad, and a simplified model of CICR must be used. Assuming that a whole-heart model is built from 10^7 individual 25-variable cell models each simulated in 0.1 seconds real time, 1 second of simulation of the whole-heart model using a 100-processor computer takes roughly 3 hours real time. Hence, such a system can run only a single 8 second simulation in a day. This demonstrates how crucial it is in computational whole-heart studies that each cell is represented by a computationally-efficient model.

The four articles included in this thesis describe CICR at four levels of detail in the cardiac dyad. The most detailed model (article III) describes realistic diffusion of Ca^{2+} ions in the cardiac dyad in the presence of electrostatic potentials and dyadic protein structures using the discretized Fokker-Planck approximation. The next level of detail is provided by article IV, in which Ca^{2+} concentration profile is in equilibrium in the cardiac dyad. This in turn can be approximated by a constant Ca^{2+} concentration in the cardiac dyad (article I). The most drastic simplification is the complete omission the cardiac dyad in a model, as was done in article II. Hence, the models of articles I-IV can be organized into a multiscale hierarchy describing CICR at four levels of detail.

6.5 Conclusions

The heart is a remarkably well-tuned system, which rapidly adapts in response to a wide variety of physiological stimuli. The applications of mathematical methods presented in this thesis are novel, and they were formulated to enable a more thorough understanding of the heart, CICR and cardiac myocytes, and to better understand their robustness. The results of this thesis show that noise modulates the functioning of a cardiac myocyte: (1) gating noise due to L-type Ca^{2+} channels gating in mode 2 may induce early after-depolarizations which trigger arrhythmias, (2) voltage noise mostly due to ion channel gating noise may increase average action potential duration,

not only variance of action potential duration, and skew distribution of action potential durations toward long durations, and (3) Ca^{2+} signaling noise due to the small number of free Ca^{2+} ions mediating CICR likely slightly reduces Excitation-Contraction coupling gain. Despite the fact that a significant Ca^{2+} signaling noise in present in CICR, it was found that at the whole-cell level Excitation-Contraction coupling is robust, partly due to the shape of RyR protein structures found in the cardiac dyad.

Appendix A

Local equilibrium approximation

Wang et al. [99] derived a local equilibrium approximation for the Fokker-Planck equation, in which electrodiffusion in a cavity is coarse-grained to random movement on a lattice. The method of Wang et al. [99] was generalized by Xing et al. [108], whose approach is followed in this Appendix.

Wang et al. [99] considered the one-dimensional Fokker-Planck equation

$$\frac{\partial \rho(t,x)}{\partial t} = \frac{\partial}{\partial x}\left[D\frac{\phi'(x)}{k_B T}\rho(t,x) + D\frac{\partial \rho(t,x)}{\partial x}\right], \qquad \rho(0,x) = F(x), \tag{A.1}$$

defined on $[a,b] \subset \mathbb{R}$. In equation (A.1), $\rho : [a,b] \to \mathbb{R}$ is the probability density of, e.g., Ca^{2+} ions, $D \in \mathbb{R}$ is the diffusion coefficient, $\phi : \mathbb{R} \to \mathbb{R}$ describes the potential energy, and $F : \mathbb{R} \to \mathbb{R}$ gives the initial probability density of ions on interval $[a,b]$. Boundaries at $\{a,b\}$ are either absorbing or reflecting. The aim is to discretize equation (A.1) to a discrete-state continuous-time Markov process.

The main idea of Wang et al. [99] was to use a finite-difference scheme that allows interpretation as a Markov process. First ρ is discretized to $p_n(t) = \int_{x_n}^{x_{n+1}} \rho(t,y)dy$ on a lattice defined by the set $\{(x_n, x_{n+1})\}_{n=1}^{N}$ of intervals with constant spacing $\Delta x = (b-a)/N$, where $x_1 = a$, $x_n = a + (n-1)\Delta x$, and $x_{N+1} = b$. Variables $p_n : \mathbb{R} \to \mathbb{R}$ evolve according to a mean-field equation

$$\frac{dp_n(t)}{dt} = \alpha_{n+1}p_{n+1}(t) + \beta_{n-1}p_{n-1}(t) - (\alpha_n + \beta_n)p_n(t) = J_n - J_{n-1}, \tag{A.2}$$

where J_n is the net probability flux between lattice points x_n and x_{n+1} defined by

$$J_n = \alpha_{n+1}p_{n+1} - \beta_n p_n. \tag{A.3}$$

In local equilibrium on $(\alpha, \beta) \subset [a, b]$, the equation (A.1) reduces to

$$0 = \frac{\partial}{\partial x}\left[D\frac{\phi'(x)}{k_B T}\rho(t,x) + D\frac{\partial \rho(t,x)}{\partial x}\right] \tag{A.4}$$

for all $x \in (\alpha, \beta)$. The general solution to equation (A.4) is

$$\rho_{\text{eq}}(x) = e^{-\phi(x)/k_B T}\left(C_1 \int_a^x e^{\phi(s)/k_B T} ds + K_1\right), \tag{A.5}$$

where $C_1, K_1 \in \mathbb{R}$ are integration constants. To derive local equilibrium jump rates, assume that ρ is in equilibrium on interval (x_{n-1}, x_{n+1}). Then jump rates between intervals $I_{n-1} = (x_{n-1}, x_n)$ and $I_n = (x_n, x_{n+1})$ can be computed from flux $J(y) = -D[\frac{\phi'(y)}{k_B T}\rho(t,y) + \frac{\partial \rho(t,y)}{\partial y}]$ at the boundary $y = x_n$ between intervals I_{n-1} and I_n. Since $\rho'_{\text{eq}}(x_n) = C_1 - \phi'(x_n)\rho(x_n)/k_B T$, flux J is in equilibrium given by $J(x_n) = -DC_1$.

Since solution (A.5) has two integration constants, two constraints are needed to fix the constants. The constraints are given by equations

$$p_{n+1} = \int_{x_n}^{x_{n+1}} \rho_{\text{eq}}(y) dy, \tag{A.6}$$

$$p_n = \int_{x_{n-1}}^{x_n} \rho_{\text{eq}}(y) dy, \tag{A.7}$$

where it is assumed that p_n and p_{n+1} are known. Solving for the integration constants, we obtain

$$C_1 = \frac{A_{n+1}p_n - A_n p_{n+1}}{A_{n+1}B_n - A_n B_{n+1}}, \tag{A.8}$$

$$K_1 = \frac{B_n p_{n+1} - B_{n+1} p_n}{A_{n+1}B_n - A_n B_{n+1}}, \tag{A.9}$$

where $A_k = \int_{x_{k-1}}^{x_k} e^{-\phi(y)/k_B T} dy$ and $B_k = \int_{x_{k-1}}^{x_k} \int_a^y e^{-(\phi(y)-\phi(z))/k_B T} dz\, dy$, where $k \in \{n, n+1\}$.

Rates α_{n+1} and β_n can be identified from flux $J(x_n)$ and from equation (A.3), and they are given by

$$\alpha_{n+1} = \frac{DA_n}{B_n A_{n+1} - B_{n+1} A_n}, \tag{A.10}$$

$$\beta_n = \frac{DA_{n+1}}{B_n A_{n+1} - B_{n+1} A_n}. \tag{A.11}$$

Equations (A.10) and (A.11) define the rates for a general non-linear potential ϕ, as in Xing et al. [108]. The rates satisfy the detailed-balance constraint,

as is shown in the following. When free energy G_n of interval (x_{n-1}, x_n) is given by

$$G_n = k_B T \ln\left(\int_{x_{n-1}}^{x_n} \exp(\frac{-\phi(y)}{k_B T})dy\right), \tag{A.12}$$

rates α_{n+1}, β_n satisfy the detailed balance equation [108]

$$\frac{\alpha_{n+1}}{\beta_n} = \frac{A_n}{A_{n+1}} = \exp(\frac{G_n - G_{n+1}}{k_B T}). \tag{A.13}$$

Hence, the process is in detailed balance by construction, which ensures that no energetically free cycles are present.

In article III, it was assumed that potential ϕ is linear, that is, $\phi(x) = sx$. Under these conditions, rates α_{n+1} and β_n are given by

$$\alpha_{n+1} = \frac{D}{(\Delta x)^2}\frac{g}{1 - e^{-g}}, \tag{A.14}$$

$$\beta_n = \frac{D}{(\Delta x)^2}\frac{g}{e^{g} - 1}. \tag{A.15}$$

where $g = s\Delta x/k_B T$. In the absence of electric potential, that is $\phi(x) = 0$, equations (A.10) and (A.11) reduce to $\alpha_{n+1} = \frac{D}{(\Delta x)^2}$ and $\beta_n = \frac{D}{(\Delta x)^2}$, that is, to pure diffusion.

Finally, we must investigate boundaries of the dyad. The assumption that the boundary at a is reflecting (that is, $\rho'(x) = 0$ on the boundary) does not change rates (A.14) and (A.15). However, when the boundary at a is absorbing (that is, $\rho(x) = 0$ on the boundary), the absorption rate is for the linear potential $\phi(x) = sx$ given by $\alpha_0 = \frac{D}{(\Delta x)^2}\frac{g^2}{e^g - 1 - g}$ [99]. This rate can be derived from equation (A.6). Boundary at b is treated in a similar way.

The method described above yields a Markov process approximating electrodiffusion. The method can be used both in a stochastic simulation and in a mean-field approach. While the above derivation was done in one dimension, the results can directly be generalized to a higher dimensional space.

Bibliography

[1] R. Adair. Noise and stochastic resonance in voltage-gated ion channels. *Proc. Natl. Acad. Sci. USA*, 100(21):12099–12104, 2003.

[2] C. Adler and U. Costabel. Cell number in human heart in atrophy, hypertrophy, and under the influence of cytostatics. *Recent Adv. Stud. Cardiac Struct. Metab.*, 6:343–55, 1975.

[3] L. Alvarez. Does increased stochasticity speed up extinction? *J. Math. Biol.*, 43(6):534–544, 2001.

[4] S. Andrews and D. Bray. Stochastic simulation of chemical reactions with spatial resolution and single molecule detail. *Physical Biology*, 1(3):137–151, 2004.

[5] C. Armstrong and F. Bezanilla. Charge movement associated with the opening and closing of the activation gates of the Na channels. *J. Gen. Physiol.*, 63(5):533–552, 1974.

[6] K. Astala and L. Päivärinta. Calderon's inverse conductivity problem in the plane. *Annals of Mathematics*, 163:265–299, 2006.

[7] K. Barstow, S. Locknar, L. Merriam, and R. Parsons. The modulation of action potential generation by calcium-induced calcium release is enhanced by mitochondrial inhibitors in mudpuppy parasympathetic neurons. *Neuroscience*, 124(2):327–339, 2004.

[8] G. Beeler and H. Reuter. Reconstruction of the action potential of ventricular myocardial fibres. *J. Physiol.*, 268(1):177–210, 1977.

[9] H. Berkefeld, C. Sailer, W. Bildl, V. Rohde, J. Thumfart, S. Eble, N. Klugbauer, E. Reisinger, J. Bischofberger, D. Oliver, et al. BKCa-Cav channel complexes mediate rapid and localized Ca^{2+}-activated K^+ signaling. *Science*, 314(5799):615, 2006.

[10] D. Bers. *Excitation-contraction coupling and cardiac contractile force.* Springer, 2001.

[11] U. Bhalla. Signaling in small subcellular volumes. I. Stochastic and diffusion effects on individual pathways. *Biophys. J.*, 87:733–744, 2004.

[12] A. Borodin and P. Salminen. *Handbook of Brownian motion: facts and formulae.* Birkhauser, 2002.

[13] A. Bortz, M. Kalos, and J. Lebowitz. A new algorithm for Monte Carlo simulation of Ising spin systems. *J. Comput. Phys*, 17(10), 1975.

[14] M. Cannell and C. Soeller. Numerical analysis of ryanodine receptor activation by L-type channel activity in the cardiac muscle diad. *Biophys. J.*, 73(1):112–122, 1997.

[15] R. Cannon and G. D'Alessandro. The ion channel inverse problem: neuroinformatics meets biophysics. *PLoS Comput. Biol.*, 2:e91, 2006.

[16] X. Chen, V. Piacentino, S. Furukawa, B. Goldman, K. Margulies, and S. Houser. L-Type Ca2+ channel density and regulation are altered in failing human ventricular myocytes and recover after support with mechanical assist devices. *Circ. Res.*, 91:517, 2002.

[17] C. Clancy and Y. Rudy. Linking a genetic defect to its cellular phenotype in a cardiac arrhythmia. *Nature*, 400:556–569, 1999.

[18] J. Clay and R. DeHaan. Fluctuations in interbeat interval in rhythmic heart-cell clusters. Role of membrane voltage noise. *Biophys. J.*, 28(3):377–389, 1979.

[19] F. Conti, L. J. DeFelice, and E. Wanke. Potassium and sodium current noise from squid axon membranes. *J. Physiol. (Lond.)*, 248:45–82, 1975.

[20] S. Cortassa, M. Aon, B. O'Rourke, R. Jacques, H. Tseng, E. Marban, and R. Winslow. A computational model integrating electrophysiology, contraction, and mitochondrial bioenergetics in the ventricular myocyte. *Biophys. J.*, 91(4):1564, 2006.

[21] J. Couzin. Drug safety: withdrawal of Vioxx casts a shadow over COX-2 inhibitors. *Science*, 306:384–5, 2004.

[22] J. Cox, F. Reimann, A. Nicholas, G. Thornton, E. Roberts, K. Springell, G. Karbani, H. Jafri, J. Mannan, Y. Raashid, L. Al-Gazali, H. Hamamy, E. Valente, S. Gorman, R. Williams, D. McHale, J. Wood, F. Gribble, and C. Woods. An SCN9A channelopathy causes congenital inability to experience pain. *Nature*, 444(5):894–8, 2006.

[23] G. De Ferrari, M. Viola, E. D'Amato, R. Antolini, and S. Forti. Distinct patterns of calcium transients during early and delayed afterdepolarizations induced by isoproterenol in ventricular myocytes. *Circulation*, 91:2510–2515, 1995.

[24] D. Difrancesco and D. Noble. A model of cardiac electrical activity incorporating ionic pumps and concentration changes. *Proc. R. Soc. B*, 307(1133):353–398, 1985.

[25] T. Dobzhansky. *Genetics of the evolutionary process.* Columbia University Press, 1971.

[26] M. Endo. Calcium release from the sarcoplasmic reticulum. *Physiological Reviews*, 57:71–108, 1977.

[27] M. Endo, M. Tanaka, and Y. Ogawa. Calcium induced release of calcium from the sarcoplasmic reticulum of skinned skeletal muscle fibres. *Nature*, 228(5266):34–36, 1970.

[28] L. Endresen. Chaos in weakly-coupled pacemaker cells. *J. Theor. Biol.*, 184(1):41–50, 1997.

[29] J. Gargus. Unraveling monogenic channelopathies and their implications for complex polygenic disease. *Am. J. Hum. Genet.*, 72(4):785–803, 2003.

[30] D. Gillespie. Exact stochastic simulation of coupled chemical reactions. *J. Phys. Chem*, 81(25):2340–2361, 1977.

[31] I. Goychuk and P. Hänggi. The role of conformational diffusion in ion channel gating. *Physica A*, 325(1-2):9–18, 2003.

[32] J. Greenstein, R. Hinch, and R. Winslow. Mechanisms of excitation-contraction coupling in an integrative model of the cardiac ventricular myocyte. *Biophys. J.*, 90(1):77–91, 2006.

[33] J. Greenstein, A. Tanskanen, and R. Winslow. Modeling the actions of β-adrenergic signaling on excitation-contraction coupling processes. *Ann. N.Y. Acad. Sci.*, 1015(1):16–27, 2004.

[34] J. Greenstein and R. Winslow. An integrative model of the cardiac ventricular myocyte incorporating local control of Ca^{2+} release. *Biophys. J.*, 83(6):2918–2945, 2002.

[35] S. Guan, Q. Lu, and K. Huang. A discussion about the DiFrancesco-Noble model. *J. Theor. Biol.*, 189(1):27–32, 1997.

[36] H. Hashitani and A. Brading. Ionic basis for the regulation of spontaneous excitation in detrusor smooth muscle cells of the guinea-pig urinary bladder. *British Journal of Pharmacology*, 140(1):159–169, 2003.

[37] P. Hess, J. Lansman, and R. Tsien. Different modes of Ca channel gating behaviour favored by dihydropyridine Ca agonists and antagonists. *Nature*, 311:538–544, 1984.

[38] B. Hille. *Ion channels of excitable membranes, 3rd edition.* Sinauer Sunderland, Massachusetts, 2001.

[39] R. Hinch, J. Greenstein, A. Tanskanen, L. Xu, and R. Winslow. A simplified local control model of calcium-induced calcium release in cardiac ventricular myocytes. *Biophys. J.*, 87(6):3723–3736, 2004.

[40] R. Hinch, J. Greenstein, and R. Winslow. Multi-scale models of local control of calcium induced calcium release. *Prog. Biophys. Mol. Biol.*, 90(1-3):136–150, 2005.

[41] A. Hodgkin and A. Huxley. A quantitative description of membrane current and its application to conduction and excitation in nerve. *J. Physiol. (Lond.)*, 117:500–544, 1952.

[42] M. Hodgson. A Bayesian restoration of an ion channel signal. *J. R. Stat. Soc. B*, 61(1):95–114, 1999.

[43] T. Hund, J. Kucera, N. Otani, and Y. Rudy. Ionic charge conservation and long-term steady state in the Luo-Rudy dynamic cell model. *Biophys. J.*, 81(6):3324–3331, 2001.

[44] P. Hunter and T. Borg. Integration from proteins to organs: the Physiome Project. *Nat. Rev. Mol. Cell. Biol.*, 4:237, 2003.

[45] P. Hunter, P. Kohl, and D. Noble. Integrative models of the heart: achievements and limitations. *Phil. Trans. R. Soc. Lond. A*, 359:1049–1054, 2001.

[46] K. Itô and H. McKean. *Diffusion processes and their sample paths.* Springer, 1974.

[47] V. Iyer, R. Mazhari, and R. Winslow. A computational model of the human left-ventricular epicardial myocyte. *Biophys. J.*, 87(3):1507–1525, 2004.

[48] A. Katz. Cardiac arrhythmias. *Advan. Physiol. Educ.*, 277:214–233, 1999.

[49] X. Koh, B. Srinivasan, H. Ching, and A. Levchenko. A 3D monte carlo analysis of the role of dyadic space geometry in spark generation. *Biophys. J.*, 90(6):1999–2014, 2006.

[50] H. Kuboniwa, N. Tjandra, S. Grzesiek, H. Ren, C. Klee, and A. Bax. Solution structure of calcium-free calmodulin. *Nat. Struct. Biol.*, 2(9):768–776, 1995.

[51] P. Laitinen. *Genetic defects of calcium and potassium signaling in inherited ventricular arrhythmias.* PhD thesis, University of Helsinki, 2004.

[52] G. Langer and A. Peskoff. Calcium concentration and movement in the diadic cleft space of the cardiac ventricular cell. *Biophys. J.*, 70(3):1169–1182, 1996.

[53] A. Lelli, P. Perin, M. Martini, C. Ciubotaru, I. Prigioni, P. Valli, M. Rossi, and F. Mammano. Presynaptic calcium stores modulate afferent release in vestibular hair cells. *J. Neurosci.*, 23(17):6894–6903, 2003.

[54] B. Lewin. *Genes VII.* Oxford University Press, New York, 2000.

[55] B. Lindner, J. Garcıa-Ojalvo, A. Neiman, and L. Schimansky-Geier. Effects of noise in excitable systems. *Physics Reports-Review Section Of Physics Letters*, 392:321–424, 2004.

[56] C. Luo and Y. Rudy. A model of the ventricular cardiac action potential. Depolarization, repolarization, and their interaction. *Circ. Res.*, 68(6):1501–1526, 1991.

[57] C. Luo and Y. Rudy. A dynamic model of the cardiac ventricular action potential. I. Simulations of ionic currents and concentration changes. *Circ. Res.*, 74(6):1071–1096, 1994.

[58] C. Luo and Y. Rudy. A dynamic model of the cardiac ventricular action potential. II. Afterdepolarizations, triggered activity, and potentiation. *Circ. Res.*, 74(6):1097–1113, 1994.

[59] E. Marbán. Cardiac channelopathies. *Nature*, 415:213–218, 2002.

[60] A. Mazur, D. Roden, and M. Anderson. Systematic administration of calmodulin antagonist W-7 or protein kinase A inhibitor H-8 prevents torsades de pointes in rabbits. *Circulation*, 100:2437–2442, 1999.

[61] E. Neher and B. Sakmann. Single-channel currents recorded from membrane of denervated frog muscle fibres. *Nature*, 260(5554):799–802, 1976.

[62] W. New and W. Trautwein. The ionic nature of slow inward current and its relation to contraction. *Pflügers Archiv European Journal of Physiology*, 334(1):24–38, 1972.

[63] D. Noble. Modelling the heart: insights, failures and progress. *BioEssays*, 24(12):1155–1163, 2002.

[64] D. Noble. Modeling the heart. *Physiology*, 19(4):191–197, 2004.

[65] D. Noble. *The music of life: biology beyond the genome*. Oxford University Press, 2006.

[66] D. Noble and Y. Rudy. Models of cardiac ventricular action potentials: iterative interaction between experiment and simulation. *Phil. Trans. R. Soc. Lond. A*, 359(1783):1127–1142, 2001.

[67] D. Noble, A. Varghese, P. Kohl, and P. Noble. Improved guinea-pig ventricular cell model incorporating a diadic space, IKr and IKs, and length-and tension-dependent processes. *Can J Cardiol*, 14(1):123–34, 1998.

[68] R. Numann and P. Negulescu. High-throughput screening strategies for cardiac ion channels. *Trends Cardiovasc. Med.*, 11(2):54–9, 2001.

[69] B. Øksendal. *Stochastic differential equations: an introduction with applications*. Springer, 2003.

[70] G. Olivetti, M. Melissari, J. Capasso, and P. Anversa. Cardiomyopathy of the aging human heart. Myocyte loss and reactive cellular hypertrophy. *Circ. Res.*, 68(6):1560–1568, 1991.

[71] B. O'Rourke, D. Kass, G. Tomaselli, S. Kaab, R. Tunin, and E. Marban. Mechanisms of altered excitation-contraction coupling in canine tachycardia-induced heart failure, I experimental studies. *Circ. Res.*, 84:562–570, 1999.

[72] P. Pak, H. Nuss, R. Tunin, S. Kaab, G. Tomaselli, E. Marban, and D. Kass. Repolarization abnormalities, arrhythmia and sudden death in canine tachycardia-induced cardiomyopathy. *J. Am. Coll. Cardiol.*, 30(2):576–584, 1997.

[73] A. Peskoff and G. Langer. Calcium concentration and movement in the ventricular cardiac cell during an excitation-contraction cycle. *Biophys. J.*, 74(1):153–174, 1998.

[74] C. Rao, D. Wolf, A. Arkin, and E. Schrödinger. Control, exploitation and tolerance of intracellular noise. *Nature*, 420:231–237, 2002.

[75] J. Rice, M. Jafri, and R. Winslow. Modeling gain and gradedness of Ca^{2+} release in the functional unit of the cardiac diadic space. *Biophys. J.*, 77(4):1871–1884, 1999.

[76] D. Russell and L. Wilkens. Use of behavioural stochastic resonance by paddle fish for feeding. *Nature*, 402:291–294, 1999.

[77] E. Saftenku, A. Williams, and R. Sitsapesan. Markovian models of low and high activity levels of cardiac ryanodine receptors. *Biophys. J.*, 80(6):2727–2741, 2001.

[78] M. Samoilov, S. Plyasunov, and A. Arkin. Stochastic amplification and signaling in enzymatic futile cycles through noise-induced bistability with oscillations. *Proc. Natl. Acad. Sci. USA*, 102(7):2310–2315, 2005.

[79] T. Shannon, F. Wang, J. Puglisi, C. Weber, and D. Bers. A mathematical treatment of integrated Ca dynamics within the ventricular myocyte. *Biophys. J.*, 87(5):3351–3371, 2004.

[80] M. Sharma, L. Jeyakumar, S. Fleischer, and T. Wagenknecht. Three-Dimensional visualization of FKBP12.6 binding to an open conformation of cardiac ryanodine receptor. *Biophys. J.*, 90(1):164–172, 2006.

[81] M. Sharma, P. Penczek, R. Grassucci, H. Xin, S. Fleischer, and T. Wagenknecht. Cryoelectron microscopy and image analysis of the cardiac ryanodine receptor. *J. Biol. Chem.*, 273(29):18429–18434, 1998.

[82] C. Soeller and M. Cannell. Numerical simulation of local calcium movements during L-type calcium channel gating in the cardiac diad. *Biophys. J.*, 73(1):97–111, 1997.

[83] L. Song, S. Wang, R. Xiao, H. Spurgeon, E. Lakatta, and H. Cheng. β-adrenergic stimulation synchronizes intracellular Ca^{2+} release during excitation-contraction coupling in cardiac myocytes. *Circ. Res.*, 88:794, 2001.

[84] T. Sridhar, M. Brown, and W. Sewell. Unique postsynaptic signaling at the hair cell efferent synapse permits calcium to evoke changes on two time scales. *J. Neurosci.*, 17(1):428–437, 1997.

[85] M. Stern. Theory of excitation-contraction coupling in cardiac muscle. *Biophys. J.*, 63(2):497–517, 1992.

[86] M. Stern and H. Cheng. Putting out the fire: what terminates calcium-induced calcium release in cardiac muscle. *Cell Calcium*, 35(6):591–601, 2004.

[87] M. Stern, L. Song, H. Cheng, J. Sham, H. Yang, K. Boheler, and E. Rios. Local control models of cardiac excitation-contraction coupling a possible role for allosteric interactions between ryanodine receptors. *J. Gen. Physiol.*, 113(3):469–489, 1999.

[88] J. Stiles, T. Bartol, and E. De Schutter. Monte Carlo methods for simulating realistic synaptic microphysiology using MCell. In: Computational Neuroscience: Realistic Modeling for Experimentalists, ed. De Schutter. pages 87–127, 2001.

[89] S. Strogatz. *Nonlinear dynamics and chaos.* Addison-Wesley, Reading, MA, 1994.

[90] A. Tanskanen, E. Tanskanen, J. Greenstein, and R. Winslow. How to formulate membrane potential in a spatially homogeneous myocyte model? *Arxiv preprint q-bio.CB/0508041*, 2005.

[91] K. ten Tusscher, D. Noble, P. Noble, and A. Panfilov. A model for human ventricular tissue. *Am. J. Physiol. Heart Circ. Physiol.*, 286(4):1573–1589, 1573.

[92] B. van der Pol and J. van der Mark. The heartbeat considered as a relaxation oscillation, and an electrical model of the heart. *Phil. Mag.*, 6:763–775, 1928.

[93] A. Varghese and G. Sell. A conservation principle and its effect on the formulation of na-ca exchanger current in cardiac cells. *J. Theor. Biol.*, 189(1):33–40, 1997.

[94] A. Varghese and R. Winslow. Dynamics of the calcium subsystem in cardiac purkinje fibers. *Physica D*, 68:364–86, 1993.

[95] A. Varghese and R. Winslow. Dynamics of abnormal pacemaking activity in cardiac Purkinje fibers. *J. Theor. Biol.*, 168(4):407–20, 1994.

[96] J. Venter, M. Adams, E. Myers, P. Li, R. Mural, G. Sutton, H. Smith, M. Yandell, C. Evans, R. Holt, et al. The sequence of the human genome. *Science*, 291:1304–1351, 2001.

[97] P. Viswanathan and Y. Rudy. Pause induced early afterdepolarizations in the long QT syndrome: a simulation study. *Cardiovasc. Res.*, 42(2):530–42, 1999.

[98] Volders, P.G. and Kulcsar, A. and Vos, M.A. and Sipido, K.R. and Wellens, H.J. and Lazzara, R. and Szabo, B. Similarities between early and delayed afterdepolarizations induced by isoproterenol in canine ventricular myocytes. *Cardiovasc. Res.*, 34:348–359, 1997.

[99] H. Wang, C. Peskin, and T. Elston. A robust numerical algorithm for studying biomolecular transport processes. *J. Theor. Biol*, 221:491–511, 2003.

[100] M. Wang, R. Collins, R. Ford, N. Berrow, A. Dolphin, and A. Kitmitto. The three-dimensional structure of the cardiac L-type voltage-gated calcium channel. *J. Biol. Chem.*, 279(8):7159–7168, 2004.

[101] S. Wang, M. Stern, E. Rios, and H. Cheng. The quantal nature of Ca^{2+} sparks and in situ operation of the ryanodine receptor array in cardiac cells. *Proc. Natl. Acad. Sci. USA*, 101(11):3979–3984, 2004.

[102] J. White, J. Rubinstein, and A. Kay. Channel noise in neurons. *J. Neurosci.*, 16:3219–3235, 2000.

[103] W. Wier, T. Egan, J. Lopez-Lopez, and C. Balke. Local control of excitation-contraction coupling in rat heart cells. *J. Physiol.*, 474(3):463–471, 1994.

[104] R. Wilders, H. Jongsma, and A. van Ginneken. Pacemaker activity of the rabbit sinoatrial node. A comparison of mathematical models. *Biophys. J.*, 60(5):1202–1216, 1991.

[105] R. Winslow, S. Cortassa, and J. Greenstein. Using models of the myocyte for functional interpretation of cardiac proteomic data. *J. Physiol.*, 563:73–81, 2005.

[106] R. Winslow, J. Rice, S. Jafri, E. Marban, and B. O'Rourke. Mechanisms of altered excitation-contraction coupling in canine tachycardia-induced heart failure, II model studies. *Circ. Res.*, 84:571–586, 1999.

[107] R. Winslow, D. Scollan, A. Holmes, C. Yung, J. Zhang, and M. Jafri. Electrophysiological modeling of cardiac ventricular function: from cell to organ. *Annu. Rev. Biomed. Eng.*, 2(1):119–155, 2000.

[108] J. Xing, H. Wang, and G. Oster. From continuum Fokker-Planck models to discrete kinetic models. *Biophys. J.*, 89(3):1551–1563, 2005.

[109] E. Yamamori, Y. Iwasaki, Y. Oki, M. Yoshida, M. Asai, M. Kambayashii, Y. Oiso, and N. Nakashima. Possible involvement of ryanodine receptor-mediated intracellular calcium release in the effect of corticotropin-releasing factor on adrenocorticotropin secretion. *Endocrinology*, 145:36–38, 2004.

[110] D. Yue, S. Herzig, and E. Marban. β-adrenergic stimulation of calcium channels occurs by potentiation of high-activity gating modes. *Proc. Natl. Acad. Sci. USA*, 87:753–757, 1990.

[111] A. Zahradnikova, I. Zahradnik, I. Györke, and S. Györke. Rapid activation of the cardiac ryanodine receptor by submillisecond calcium stimuli. *J. Gen. Physiol.*, 114(6):787–798, 1999.

[112] M. Zaniboni, A. Pollard, L. Yang, and K. Spitzer. Beat-to-beat repolarization variability in ventricular myocytes and its suppression by electrical coupling. *Am. J. Physiol. Heart Circ. Physiol.*, 278(3):677–687, 2000.

[113] J. Zeng and Y. Rudy. Early afterdepolarizations in cardiac myocytes: mechanism and rate dependence. *Biophys. J.*, 68(3):949–964, 1995.

Original Articles

Article I

Article II

Article III

Article IV